Open
ORIGINAL ARTICLE

Cell Research (2014) 24:513-531.

www.nature.com/cr

Human colorectal cancer-specific *CCAT1-L* lncRNA regulates long-range chromatin interactions at the *MYC* locus

Jian-Feng Xiang[1], Qing-Fei Yin[1], Tian Chen[1], Yang Zhang[1], Xiao-Ou Zhang[2], Zheng Wu[1], Shaofeng Zhang[1], Hai-Bin Wang[3], Junhui Ge[3], Xuhua Lu[3], Li Yang[2], Ling-Ling Chen[1]

[1]State Key Laboratory of Molecular Biology, Institute of Biochemistry and Cell Biology, [2]Key Laboratory of Computational Biology, CAS-MPG Partner Institute for Computational Biology, Shanghai Institutes for Biological Sciences, Chinese Academy of Sciences, 320 Yueyang Road, Shanghai 200031, China; [3]Changzheng Hospital, Second Military Medical University, 415 Fengyang Road, Shanghai 200003, China

The human 8q24 gene desert contains multiple enhancers that form tissue-specific long-range chromatin loops with the *MYC* oncogene, but how chromatin looping at the *MYC* locus is regulated remains poorly understood. Here we demonstrate that a long noncoding RNA (lncRNA), *CCAT1-L*, is transcribed specifically in human colorectal cancers from a locus 515 kb upstream of *MYC*. This lncRNA plays a role in *MYC* transcriptional regulation and promotes long-range chromatin looping. Importantly, the *CCAT1-L* locus is located within a strong super-enhancer and is spatially close to *MYC*. Knockdown of *CCAT1-L* reduced long-range interactions between the *MYC* promoter and its enhancers. In addition, *CCAT1-L* interacts with CTCF and modulates chromatin conformation at these loop regions. These results reveal an important role of a previously unannotated lncRNA in gene regulation at the *MYC* locus.

Keywords**:** *CCAT1-L* lncRNA; super-enhancer; chromatin looping; *MYC*; CTCF
Cell Research (2014) **24**:513-531. doi:10.1038/cr.2014.35; published online 25 March 2014

Introduction

The increased sensitivity of experimental assays has revealed that long noncoding RNAs (lncRNAs) impact a variety of important biological processes (reviewed in [1, 2]). Aberrant expression of lncRNAs has been linked to cancers with distinct modes of action (reviewed in [3]). For example, *HOTAIR* is highly expressed in breast tumors and has been reported to promote cancer metastasis by targeting chromatin repressor Polycomb proteins to specific genomic loci [4]. *LincRNA-p21* in association with hnRNP-K serves as a repressor in p53-dependent transcriptional responses [5] or suppresses target mRNA translation in coordination with the RNA-binding protein HuR [6]. *MALAT1* has been implicated in the regulation of cell growth and tumor metastasis [7, 8]. These findings suggest that lncRNAs may serve as important regulators in tumorigenesis although the expression regulation of lncRNAs in specific human tumors and their mechanisms involved in tumorigenesis remain to be explored.

Enhancers are a class of DNA regulatory sequences that can activate gene expression independent of their proximity or orientation to their target genes [9]. Enhancers often form long-range chromatin loops with their target genes to control temporal- and tissue-specific gene expression during development and their mis-regulation contributes to human diseases [10]. A large portion of enhancers can be transcribed into enhancer RNAs (eRNAs) [11], which have been proposed to contribute to gene activation [12-16]. In addition, super-enhancers were recently identified and shown to consist of large clusters of transcriptional enhancers formed by binding of master transcription factors/mediators and to be associated with genes that control and define cell identity [17, 18]. Thus,

Correspondence: Ling-Ling Chen
E-mail: linglingchen@sibcb.ac.cn
Received 17 December 2013; revised 6 January 2014; accepted 27 January 2014; published online 25 March 2014

it would be interesting to know whether super-enhancers are transcribed and whether they are regulated by RNA transcripts.

The expression of the human *MYC* oncogene is complex and is regulated at multiple levels, including enhancers, promoters, transcription factors and chromatin state [17, 19-21]. The human 8q24 region includes a gene desert containing enhancers forming chromatin loops with the *MYC* promoter located several hundred kilobases telomerically. These chromatin interactions are tissue-specific in prostate, breast and colorectal cancers [19]. In colorectal cancer (CRC), one well-characterized loop is between a locus 335 kb upstream of *MYC* (*MYC*-335) and the *MYC* promoter. *MYC*-335, the site harboring an important CRC risk SNP (rs6983267), is a transcriptional enhancer that promotes the binding of transcription factor 4 (TCF4) specifically in CRC [22, 23]. Importantly, mice lacking *MYC*-335 were resistant to intestinal tumors, although *MYC* transcripts were only modestly reduced [24]. Very recently, the region upstream of *MYC* has been reported to contain an exceptionally large super-enhancer [17] and such a super-enhancer is tumor type specific in cancer cells, but not in its healthy counterparts [20]. However, how these chromatin loops at the 8q24 *MYC* locus are regulated remains unknown.

Human 8q24 has recently been reported to express several lncRNAs in different human tumors. *PRNCR1* (8q24) [25] binds to the androgen receptor (AR) and is involved in the AR-mediated gene activation in prostate cancers [26]. However, it is not expressed in CRC (Supplementary information, Figure S1). Instead, two other CRC-specific lncRNAs transcribed from 8q24 were recently reported. *CCAT1* (*Colorectal Cancer Associated Transcript 1*) is 2 600 nt in length and is a highly specific marker for CRC [27], and its upregulation is evident in both pre-malignant conditions and through all disease stages in CRC [28]. *CCAT2*, a 340 nt ncRNA transcribed from the *MYC-335* region, appeared to enhance invasion and metastasis through MYC-regulated miRNAs *miR-17-5p* and *miR-20a* [29]. However, we have been unable to detect *CCAT2* in any human CRC tissue samples or CRC-derived cell lines examined (Supplementary information, Figure S1).

Here we report that a novel 5 200 nt CRC-specific lncRNA, *CCAT1-L* (*CCAT1, the Long isoform*), is transcribed from a locus 515 kb upstream of *MYC* (*MYC*-515), a super-enhancer region of *MYC* [17, 20], and plays a role in *MYC* transcriptional regulation. We demonstrate that *CCAT1-L* localizes to its site of transcription and functions in the maintenance of chromatin looping between the *MYC* promoter and its enhancers in coordination with CTCF. Together, these results reveal a novel connection between the chromatin organization regulated by a lncRNA and *MYC* expression in a specific human cancer.

Results

CCAT1-L, a novel CRC-specific lncRNA, is abundantly transcribed from a locus 515 kb upstream of MYC on 8q24

By sequencing paired CRC/control mucosa samples from a Chinese patient, we have identified a previously unreported lncRNA, *CCAT1-L*, that is abundantly and specifically expressed in CRC (Supplementary information, Table S1 and Figure S1). *CCAT1-L* is transcribed from 8q24.21 — 515 kb upstream of the *MYC* locus (*MYC*-515) (Figure 1A). It is 5 200 nt in length, contains two exons and is polyadenylated as revealed by oligo (dT) selection followed by northern blot (Supplementary information, Figure S2A). 3′ RACE further confirmed its 3′ end and the splicing between the two exons (Supplementary information, Figure S1A and data not shown). Interestingly, *CCAT1*, a 2 600 nt lncRNA identified using Representational Difference Analysis (RDA) and cDNA cloning [27], was shown to be highly associated with pre-malignant as well as all disease stages in colon cancer tumorigenesis [27, 28]. Importantly, *CCAT1-L* that we identified here overlaps with *CCAT1* (Figure 1A and 1B), suggesting a positive correlation of *CCAT1-L* expression with colon cancer. For clarity, we refer the 2 600 nt *CCAT1* as *CCAT1-S* throughout this study.

We further confirmed extensive transcription of *CCAT1-L* in CRC tissue samples from several other patients by northern blots and *CCAT1-L*-specific RT-qPCR (Figure 1C and 1D). Consistent with the expression pattern of *CCAT1-S* [27], the expression of *CCAT1-L* is undetectable or very low in paired mucosa samples (Figure 1C and 1D) and other normal human tissue samples (Supplementary information, Figure S2B). The same northern blot probe also recognizes *CCAT1-S*, but *CCAT1-S* is expressed at a much lower level compared to *CCAT1-L* in human CRC patient tissue samples examined (Figure 1C). In addition, we observed that *CCAT1-L* is specifically expressed in cultured CRC-derived cell lines, such as HCT116, HT29 and SW48 (Figure 1E). Finally, sequence conservation analysis revealed that *CCAT1-L* is human specific and no ortholog was seen in other species examined (data not shown).

The human 8q24 gene desert region has recently been shown to express distinct lncRNAs in different human tumors [25, 27, 29] (Supplementary information, Figure S1B). However, these lncRNAs were undetectable in the sequencing data of paired CRC/control mucosa samples

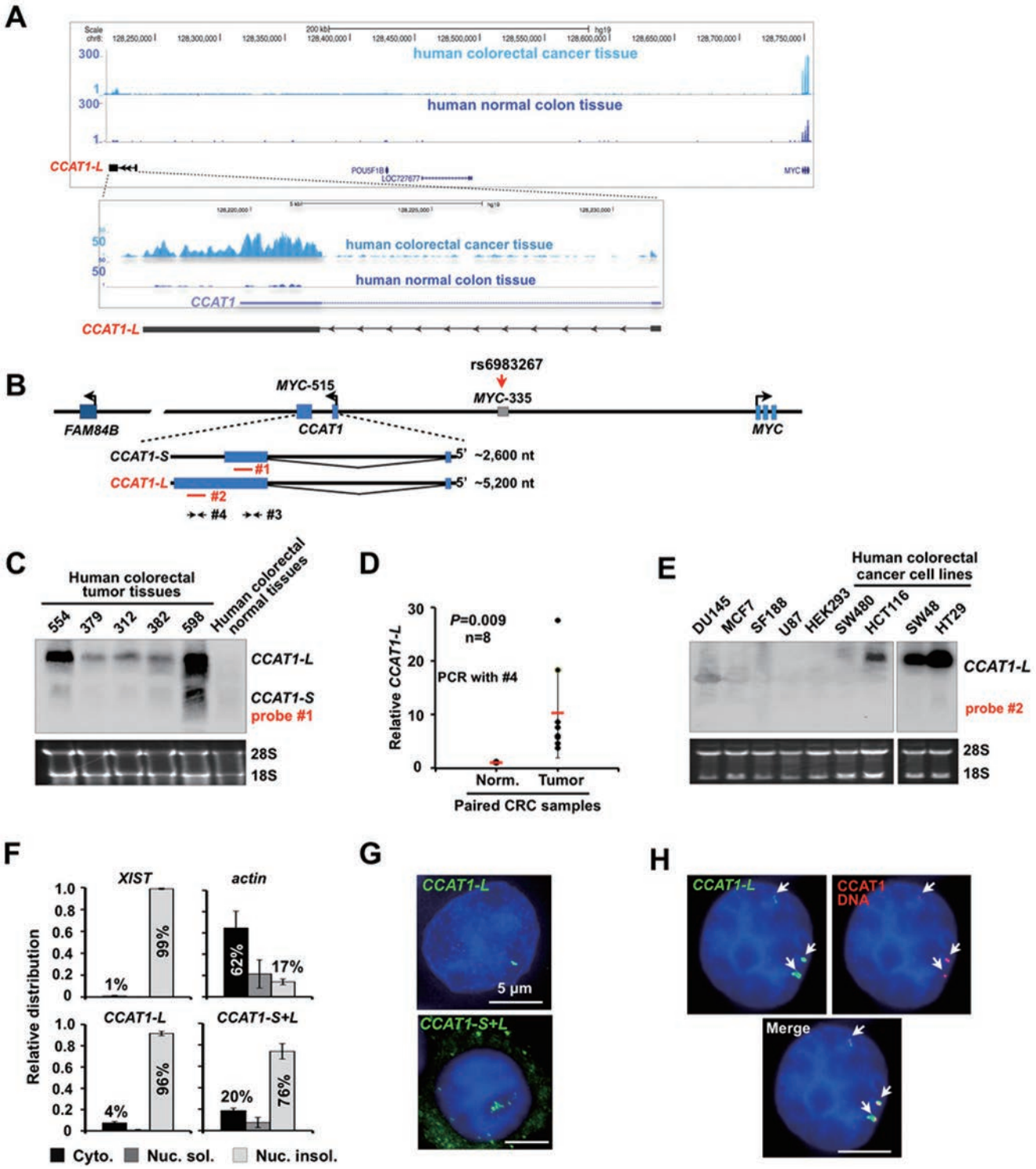

(Supplementary information, Table S1 and Figure S1C), or could not be detected in the CRC-derived cell lines that we examined (Supplementary information, Figure S1D). Thus, the significance and functional implications of these RNAs in CRC remain unclear.

CCAT1-L is a nuclear-retained lncRNA

As the two *CCAT1* isoforms overlap, we decided to characterize them in greater detail. First, both RNAs are polyadenylated (Supplementary information, Figure S2A), with halflife of about 6-8 h in HT29 cells (data

Figure 1 *CCAT1-L*, a nuclear-retained lncRNA, is specifically expressed in human CRC tissue samples. **(A)** RNA-seq of paired CRC/control mucosa samples from a Chinese patient revealed that a novel lncRNA, *CCAT1-L*, is transcribed from a locus 515 kb upstream of the *MYC* locus (*MYC*-515) on 8q24. Note that we refer the previously annotated 2 600 nt *CCAT1* as *CCAT1-S* throughout this study [27]. **(B)** A schematic view of *CCAT1* locus and its adjacent genomic information on 8q24. The locus 335 kb upstream of the *MYC* locus (*MYC*-335) contains an enhancer and a CRC risk SNP [22, 23]. Red lines denote antisense (AS) probes recognizing either both *CCAT1* isoforms (#1) or only *CCAT1-L* (#2) in northern blot; arrows denote PCR primer sets that recognize either both *CCAT1* isoforms (#3) or only *CCAT1-L* (#4). **(C)** Northern blot validated *CCAT1-L* expression in human CRC patient samples. **(D)** The relative expression of *CCAT1-L* in CRC tissues and paired control mucosa samples from the same patients. The primer sets only recognizing *CCAT1-L* was used (#4 in **B**). *P* values from one-tailed *t*-test in the pairwise comparison are shown. **(E)** Northern blot confirmed *CCAT1-L* expression in human CRC cell lines. **(F)** *CCAT1-L* is associated with the nuclear insoluble fractions. Total RNAs from HT29 cells were separated into cytoplasmic, nuclear soluble, and nuclear insoluble fractions. Bar plots represent relative abundance of RNAs in the nuclear soluble and insoluble fractions as measured by RT-qPCR. #3 or #4 described in **B** were used to detect either both *CCAT1* isofroms or *CCAT1-L* only. Error bars represent standard deviation (± SD) in triplicate experiments. **(G)** *CCAT1-L* is exclusively nuclear retained, while *CCAT1-S* is cytoplasmically distributed. RNA ISH (green) was performed with Dig-labeled probes **(B)** either recognizing *CCAT1-L* (top panel) or both isoforms of *CCAT1* (bottom panel) in HT29 cells. **(H)** *CCAT1-L* accumulates at its site of transcription. Double FISH of *CCAT1-L* (green) and its adjacent DNA region (red). A single Z stack of representative images acquired with an Olympus IX70 DeltaVision Deconvolution System microscope is shown. DAPI is in blue and the white scale bar in all images denotes 5 μm. Representative images are shown **(G**, **H)**. In **C** and **E**, 18S and 28S rRNAs were used as loading controls. Supportive data are included in Supplementary information, Figures S1 and S2.

not shown). Second, knockdown of *CCAT1-L* by an optimized phosphorothioate-modified antisense oligodeoxynucleotide (ASO) led to the simultaneous disruption of *CCAT1-S* (Supplementary information, Figure S2C), suggesting that the short isoform may be derived from *CCAT1-L*. Further analysis revealed alternative polyadenylation (APA) sites in *CCAT1-L* at a genomic position close to the 3′ end of *CCAT1-S* (data not shown). Third, we observed that *CCAT1-S* and *CCAT1-L* are localized to different subcellular compartments. By nuclear/cytoplasmic RNA fractionation, we found that *CCAT1-L* shows an association with chromatin as tight as *Xist*, a lncRNA that regulates chromatin compaction during X-chromosome inactivation [30] (Figure 1F). Fractions with both *CCAT1* isoforms revealed a less tight association of these RNAs with chromatin (Figure 1F), suggesting that *CCAT1-S* is cytoplasmic. This was further confirmed by RNA *in situ* hybridization (ISH) with probes that either detect *CCAT1-L* only or both *CCAT1* isoforms. *CCAT1-L* is exclusively located in the nucleus and accumulates in striking nuclear foci in CRC cell lines examined (Figure 1G, top panel, and data not shown). In contrast, when a probe recognizing both isoforms of *CCAT1* was used in the ISH, we found that fluorescent signals appeared in both cytoplasm and nucleus (Figure 1G, bottom panel), suggesting that *CCAT1-S* is located in the cytoplasm. This is in agreement with the previous report that *CCAT1-S* is a cytoplasm-located lncRNA [31]. Finally, we found that the nuclear-retained *CCAT1-L* does not colocalize with marker proteins of known nuclear bodies, including Cajal bodies, paraspeckles, nuclear speckles and PML bodies (data not shown). However, double DNA/RNA FISH (Figure 1H) clearly revealed that *CCAT1-L* accumulates at or near its site of transcription, suggesting a possible role of *CCAT1-L* in local gene expression or chromatin organization.

Knockdown of CCAT1-L reduces MYC expression

The *in cis* accumulation of *CCAT1-L* suggests a possible role in local gene expression. As only a few genes are expressed from the 8q24 region (Figure 1A and Supplementary information, Figure S1B), we examined the relative expression of their steady-state mRNAs after knockdown of *CCAT1-L*. While knockdown of *CCAT1-L* by ASO had no effect on the expression of *FAM84B*, which is located 667 kb centromeric to *CCAT1-L*, it led to modestly reduced expression of *MYC*, which is located 515 kb telomeric to *CCAT1-L*, as revealed by both RT-PCR and northern blot in HT29 cells (Figure 2A and 2B). In addition, we noticed a reduction of MYC protein after *CCAT1-L* ASO treatment (Figure 2B). This reduction was also observed at different times after the ASO treatment (data not shown) and in another CRC cell line HCT116 (Figure 2A). Importantly, we found that knockdown of *CCAT1-L* greatly reduced the transcription of nascent *MYC* RNA (Figure 2C), further suggesting that *CCAT1-L* regulates *MYC* expression at the transcriptional level. Nevertheless, while the reduction on the steady-state *MYC* mRNA that we observed was modest, it is possible that this at least partly reflects the known complexity of *MYC* regulation [21].

We next expressed *CCAT1-L* from a plasmid expression vector to see whether it could raise *MYC* expression. However, we observed that transient overexpression of

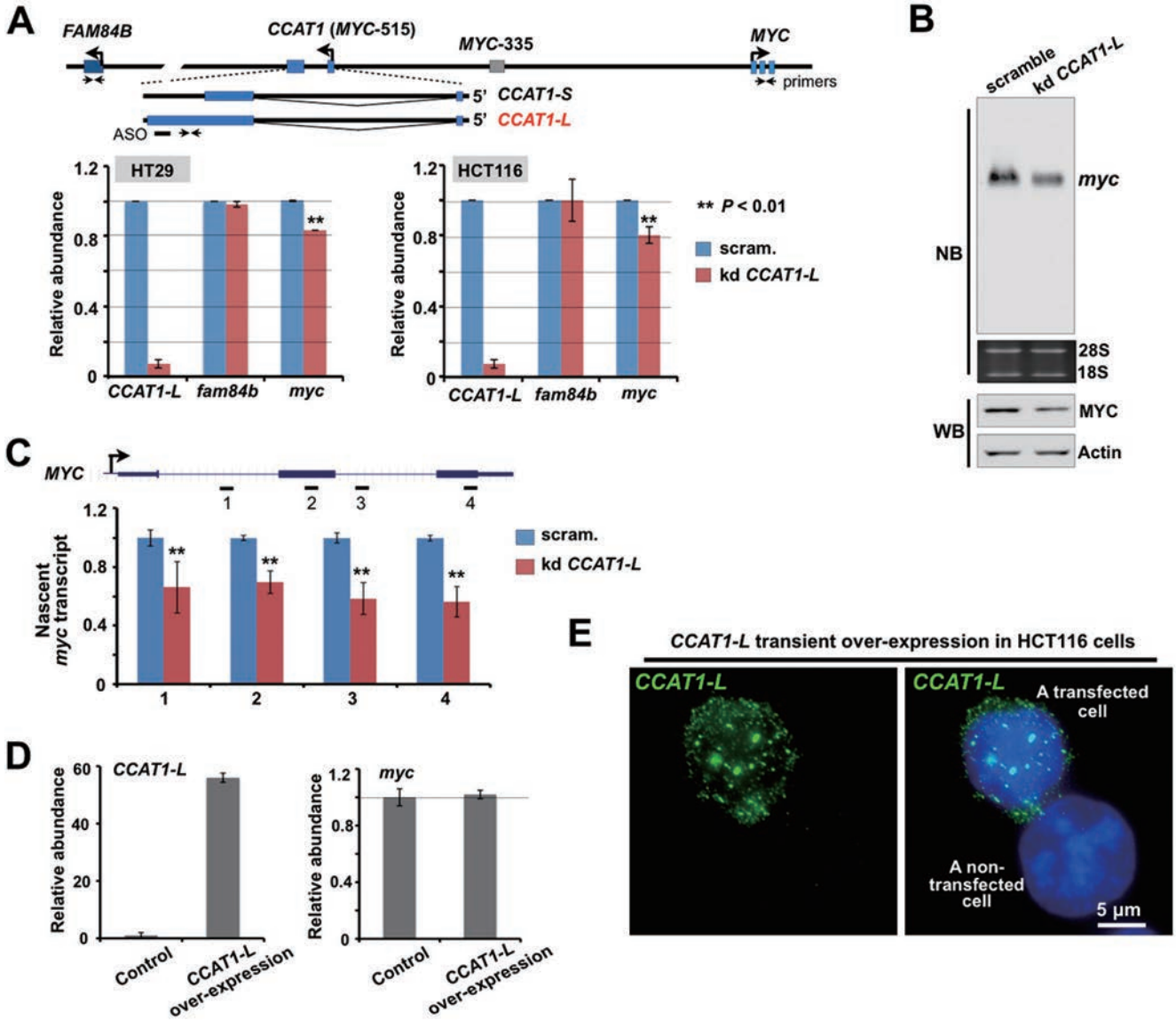

Figure 2 *CCAT1-L* regulates *MYC* expression *in cis*. **(A)** Knockdown of *CCAT1-L* led to modestly reduced expression of *MYC* in both HT29 and HCT116 cells. Top, bars represent ASO and arrows represent primer sets. Bottom, bar plots represent relative expression of *CCAT1-L*, *MYC* and *FAM84B* 36 h post the ASO treatment (normalized to *actin*). **(B)** Northern blot and western blot (WB) revealed the reduced expression of *MYC* after knockdown of *CCAT1-L* in HT29 cells. Actin was used as a loading control in WB. **(C)** *CCAT1-L* regulates *MYC* expression at the transcriptional level. A crude preparation of nuclei was subjected to nuclear run-on assay under the indicated conditions in HT29 cells. Nascent transcription of *MYC* detected from scramble ASO-treated nuclei was defined as one. **(D)** Overexpression of *CCAT1-L in trans* in expression vector resulted in no apparent activation of *MYC*. Left, RT-qPCR validated the increased expression of *CCAT1-L* in the pEGFP-C1 vector in HCT116 cells. Right, the overexpression of *CCAT1-L* in HCT116 cells did not lead to increase of *MYC* expression, as revealed by RT-qPCR. **(E)** Overexpression of *CCAT1-L* in vectors resulted in aberrant localization in the nucleus. RNA ISH (green) was performed with a probe recognizing *CCAT1-L* (**Figure 1B**) in HCT116 cells transfected with the *CCAT1-L*-expressing vector. Note that the overexpressed *CCAT1-L* produced from transfection vectors assembled as numerous nuclear dots. Representative images are shown. Scale bar, 5 μm. Error bars in **A**, **C** and **D** represent ± SD in triplicate experiments. In **A** and **C**, *P* values from one-tailed *t*-test in the pairwise comparison are shown.

CCAT1-L in trans resulted in no apparent activation of *MYC* (Figure 2D) and that the overexpressed *CCAT1-L* from the expression vector localizes to numerous nuclear sites (Figure 2E) rather than to its endogenous *in cis* site

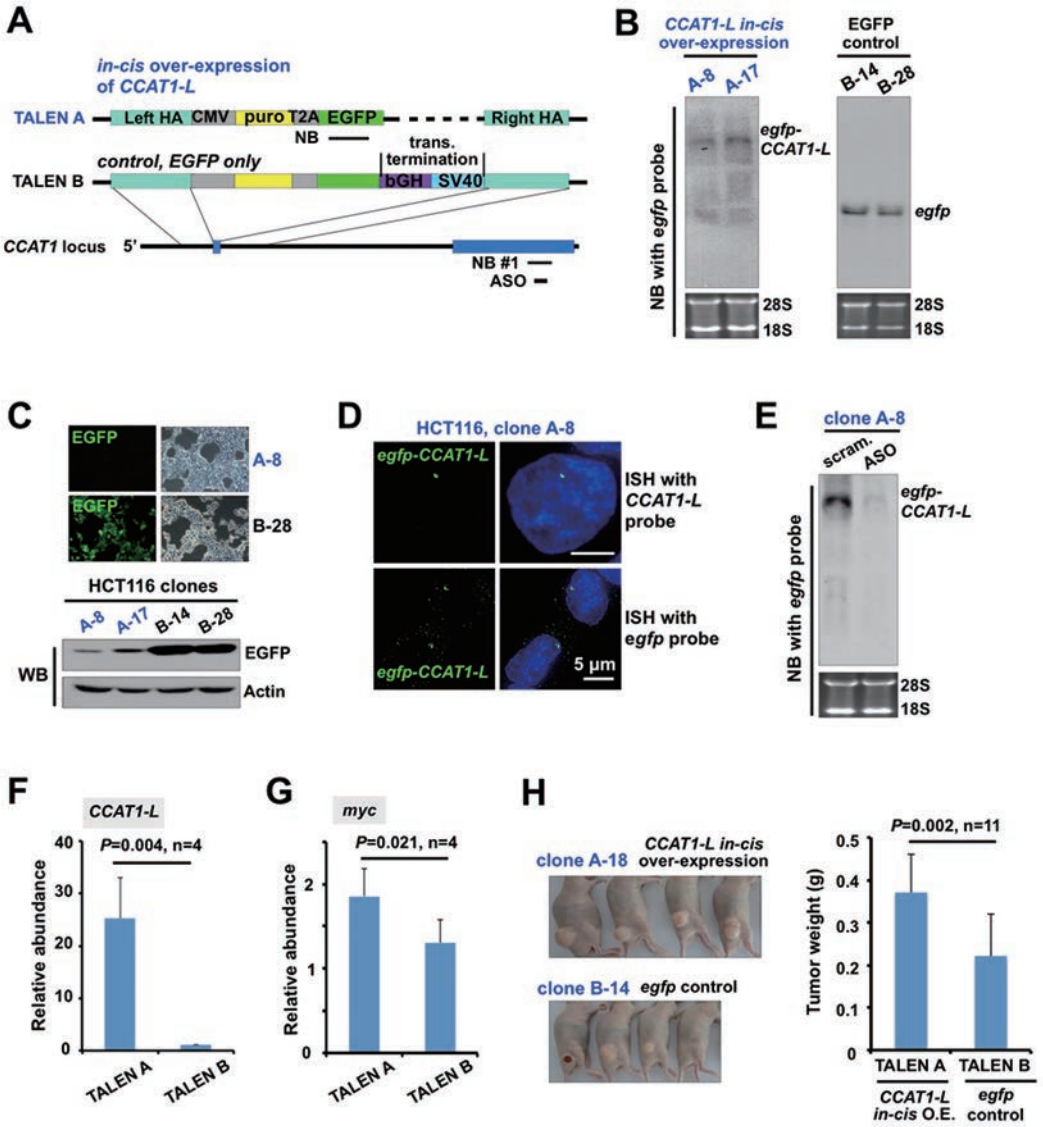

of accumulation (Figure 1H). This lack of effect was not surprising, given that regulation of *CCAT1-L* on *MYC* may require an *in-cis* action. Also, we have previously reported that other nuclear-retained lncRNAs, when expressed from transfected vectors, did not localize to the sites of their genomic counterpart regions [32, 33] or exert their roles *in cis* [33].

In cis overexpression of CCAT1-L enhances MYC expression and promotes tumorigenesis

Recently developed targeted genome-editing technologies using engineered nucleases, such as transcription activator-like effector nucleases (TALENs), provide a precise way to manipulate chromatin regions of interest (reviewed in [34]). We therefore applied TALENs to achieve *in cis* overexpression of *CCAT1-L* in HCT116 cells, which normally express a low level of *CCAT1-L* (Figure 1E). We inserted a CMV promoter and *egfp* just upstream of the *CCAT1* genomic locus to achieve a single allele insertion to express the fusion *egfp-CCAT1-L* RNA *in cis* (Figure 3A and Supplementary information, Figure S3A and S3B, TALEN A). As it has been shown that the insertion of a double poly(A) site cassette into the genome by zinc finger nucleases (ZNF) led to an efficient transcriptional stop [35], we inserted such a double poly(A) site cassette downstream of *egfp* to terminate the transcription of *CCAT1-L* at the same genomic locus to obtain the control cell line (Figure 3A, Supplementary information, Figure S3A and S3C, TALEN B). Thus, these two TALEN-engineered cell lines offered a convenient system to allow transcription of either *egfp-CCAT1-L* (TALEN A) or *egfp* (TALEN B) from the same pro-

Figure 3 *In cis* overexpression of *CCAT1-L* enhances *MYC* expression and tumorigenesis. **(A)** A schematic view of the strategy to *in cis* express *CCAT1-L* in HCT116 cells by TALEN. TALEN A, the *CCAT1-L in cis* overexpression cell line. A cassette of CMV promoter and sequences of puromycin and *egfp* mRNAs was inserted just upstream of the first exon of *CCAT1* by TALEN. TALEN B, the control cell line that overexpresses *egfp*. The same cassette of TALEN A but with two additional poly(A) sites to terminate the transcription downstream of *egfp* was inserted into the same genomic location as that in TALEN A (see Supplementary information, Figure S3 for details). Note that the transcription occurred in both *egfp-CCAT1-L*- and *egfp*-overexpressing cell lines. **(B)** Northern blot validated the overexpression of *egfp-CCAT1-L* (left panel) or *egfp* (right panel) in different TALEN lines by using a probe recognizing *egfp* shown in **A**. **(C)** *In cis* overexpressed *egfp-CCAT1-L* **(B)** was poorly translated into EGFP due to its nuclear retention, while the overexpressed *egfp* was efficiently translated into EGFP. Fluorescence microscopy (top) and WB (bottom) of representative TALEN A or TALEN B lines are shown. **(D)** Nuclear-retained *egfp-CCAT1-L* exclusively accumulated as a single nuclear dot, as revealed by ISH probes recognizing either *CCAT1-L* or *egfp* in the representative TALEN A clone. **(E)** Northern blot validated that *egfp-CCAT1-L* can be efficiently knocked down by the ASO that targets *CCAT1-L*, assayed with a probe recognizing *egfp*. **(F)** RT-qPCR revealed the overexpression of *CCAT1-L* in TALEN A lines, but not in control TALEN B lines (normalized to *actin* and the non-engineered HCT116 cells). Four lines of TALEN A and TALEN B cells were analyzed individually. **(G)** *In cis* overexpression of *egfp-CCAT1-L* enhanced *MYC* expression, as revealed by RT-qPCR (normalized to *actin* and the non-engineered HCT116 cells). The same lines of TALEN A and TALEN B cells in **F** were analyzed. **(H)** *In cis* overexpression of *egfp-CCAT1-L* increased tumor formation in a mouse xenograft model. Xenograft tumors were collected 4 weeks after inoculation of cells. Left, representative xenograft tumors generated from a TALEN A and a TALEN B line are shown. Right, comparison was made between the *egfp-CCAT1-L in cis* overexpressing TALEN A lines and the *egfp in cis* overexpressed TALEN B lines. Note that xenograft tumors raised from individual *in cis egfp-CCAT1-L*-overexpressing HCT116 cell lines were larger than those raised from control TALEN-engineered cell lines. Error bars in **F**-**H** represent ± SD in indicated multiple experiments. *P* values from one-tailed *t*-test in the pairwise comparison are shown. 18S and 28S rRNAs were used as loading controls in all northern blots. Supportive data are included in Supplementary information, Figures S1-S4.

moter *in cis*. However, using similar approaches we have been unable to obtain complete knockdown of *CCAT1-L*, owing to amplification and hence multiple alleles of this locus in CRC lines.

As expected, with a northern blot probe that recognizes *egfp*, we found that *egfp-CCAT1-L* or *egfp* was expressed in the indicated TALEN lines (Figure 3B). Importantly, we observed that *egfp-CCAT1-L* was rarely exported to the cytoplasm for EGFP translation (Figure 3C, 3D and Supplementary information, Figure S3D), further confirming that it is a nuclear-retained lncRNA. In contrast, all control TALEN lines that only express *egfp* resulted in a strong EGFP fluorescence (Figure 3C and Supplementary information, Figure S3D). In addition, the expression of *egfp-CCAT1-L* was further confirmed by a northern blot probe that recognizes *CCAT1* (Supplementary information, Figure S3E), while no overexpressed *CCAT1-L* was detected in the *egfp*-expressing control TALEN lines (Supplementary information, Figure S3F), suggesting that the transcriptional terminator after *egfp* is efficient. The *egfp-CCAT1-L* TALEN lines achieved a 15-30-fold increase in *in cis* expression of *CCAT1-L*, while *CCAT1-L* expression remained low in *egfp*-overexpressing control TALEN lines (Figure 3F and Supplementary information, Figure S3E and S3F). Finally, we found that the overexpressed *egfp-CCAT1-L* was not efficiently processed to *CCAT1-S*, as only the long isoform of *CCAT1* appeared in all northern blots (Figure 3B, 3E and Supplementary information, Figure S3E). Although these results suggest that the biogenesis of two isoforms of *CCAT1* requires further attention, they also reveal that the *in cis* overexpression offers a clear system to evaluate the function of *CCAT1-L* in the current study.

Importantly, *egfp-CCAT1-L* can also be knocked down by the same ASO that targets *CCAT1-L*, as revealed by northern blot with an *egfp* probe (Figure 3E). Furthermore, this ASO treatment also led to a consistent reduction of *MYC* transcripts in several *in cis CCAT1-L*-overexpressing HCT116 cell lines (Supplementary information, Figure S4A). It is worth noting that the *in cis* activated *egfp-CCAT1-L* RNA does not colocalize to known nuclear bodies (Supplementary information, Figure S4B), but instead locates as one single nuclear accumulation (Figure 3D) to its site of transcription (Figure 4E). These characteristics of *egfp-CCAT1-L* resemble known molecular features of the endogenous *CCAT1-L* (Figure 1F-1H).

Compared to the control engineered TALEN B HCT116 cells (Figure 3A), the *in cis* overexpressed *egfp-CCAT1-L* enhanced *MYC* expression (Figure 3G). Furthermore, we also observed that *egfp-CCAT1-L*-overexpressing HCT116 cells grew faster than the control cell lines under low serum culture conditions (data not shown). Moreover, transplantation of *egfp-CCAT1-L*-overexpressing HCT116 cell lines resulted in larger xenograft tumors in nude mice when compared to *egfp*-overexpressing con-

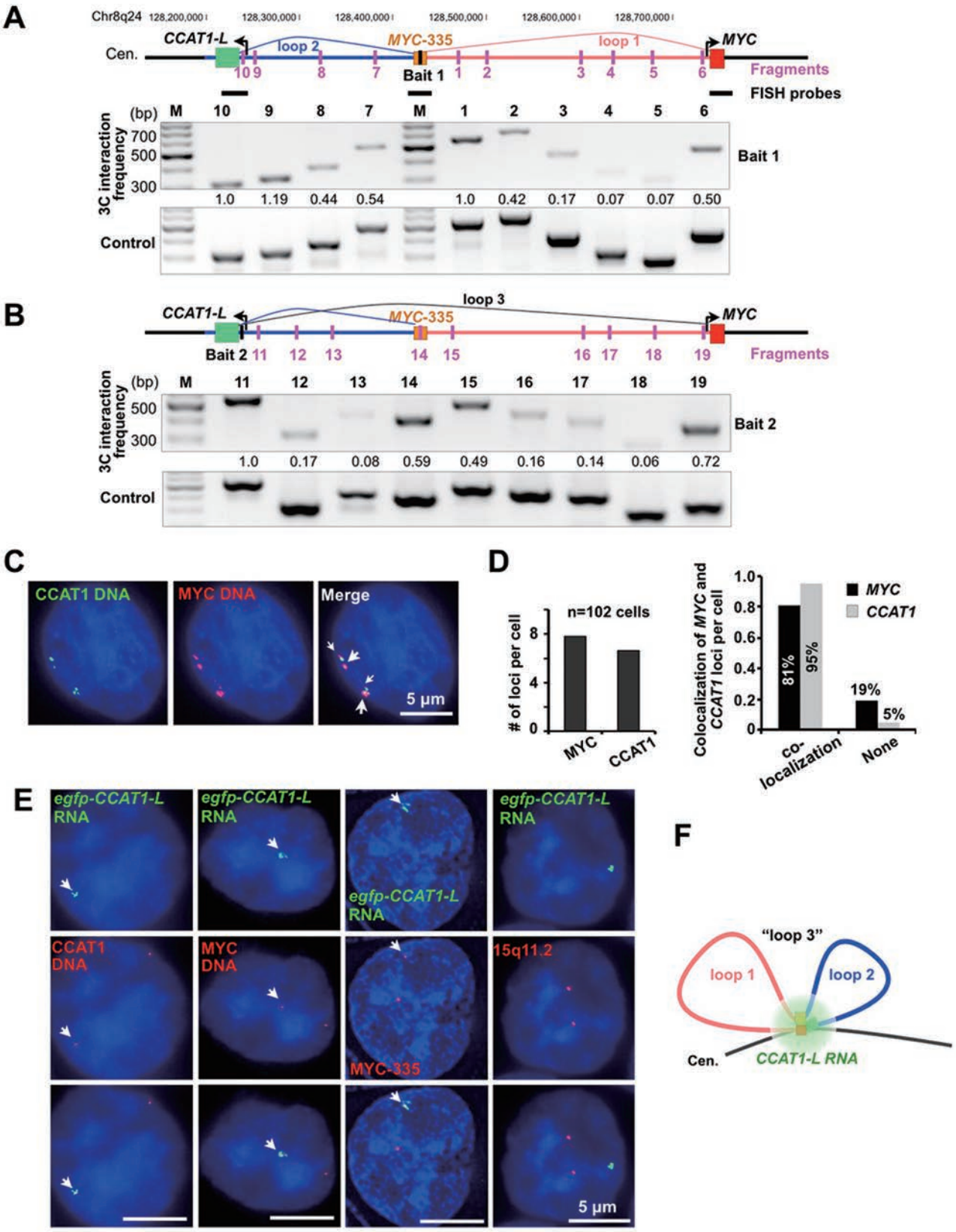
A
Chr8q24 128,200,000 128,300,000 128,400,000 128,500,000 128,600,000 128,700,000
CCAT1-L
Cen.
loop 2
MYC-335
loop 1
MYC
10 9 8 7 Bait 1 1 2 3 4 5 6
Fragments
FISH probes
(bp) M 10 9 8 7 M 1 2 3 4 5 6
3C interaction frequency
700
500
300
Bait 1
1.0 1.19 0.44 0.54 1.0 0.42 0.17 0.07 0.07 0.50
Control
B
loop 3
CCAT1-L
MYC-335
MYC
Bait 2 11 12 13 14 15 16 17 18 19
Fragments
(bp) M 11 12 13 14 15 16 17 18 19
3C interaction frequency
500
300
Bait 2
1.0 0.17 0.08 0.59 0.49 0.16 0.14 0.06 0.72
Control
C
CCAT1 DNA
MYC DNA
Merge
5 μm
D
n=102 cells
# of loci per cell
8
4
0
MYC
CCAT1
Colocalization of MYC and CCAT1 loci per cell
1.0
0.8
0.6
0.4
0.2
0
MYC
CCAT1
81%
95%
19%
5%
co-localization
None
E
egfp-CCAT1-L RNA
egfp-CCAT1-L RNA
egfp-CCAT1-L RNA
egfp-CCAT1-L RNA
CCAT1 DNA
MYC DNA
MYC-335
15q11.2
5 μm
F
"loop 3"
loop 1
loop 2
Cen.
CCAT1-L RNA

Figure 4 The long-range interaction between the *MYC* promoter and its upstream regulatory elements. **(A)** The existence of multiple chromatin loops in the upstream region of *MYC* in HT29 cells. Physical map of the region spanning a 550 kb distance with *CCAT1-L* (*MYC*-515) at one end and *MYC* at the other, interrogated by 3C. Top, the position of the constant fragment containing *MYC*-335, a known region that is looping with the *MYC* promoter [22], is marked by a black bar (bait 1); positions of *Hind*III restriction target fragments are marked by pink bars and primers were designed accordingly. Bottom, 3C interaction frequencies of the constant fragment with other fragments revealed the increased interaction between *MYC*-335 and *MYC* promoter and between *MYC*-335 and *MYC*-515. 3C products were confirmed by Sanger sequencing (examples were shown in Supplementary information, Figure S5B). The relative abundance of each 3C PCR product was determined using ImageJ, normalized by each corresponding input signal and the bait PCR product (set as 1.0), and labeled underneath. **(B)** The chromatin loops in the upstream region of *MYC*. Top, the position of the constant fragment containing *CCAT1-L* locus (*MYC*-515) is marked by a black bar (bait 2); see **A** for details. **(C)** Double DNA FISH of *CCAT1-L* (green) and *MYC* (red) genomic loci in HT29 cells. FISH probes are labeled as black bars in **A**. White arrows indicate the co-localized loci from a representative cell. **(D)** The majority of *CCAT1-L* and *MYC* genomic regions are spatially close. Left, each HT29 cell contains multiple *CCAT1-L* and *MYC* loci, and the number of each locus per cell was calculated from totally 102 cells counted. Right, the majority of *CCAT1-L* loci in HT29 cells co-localize with *MYC* loci. **(E)** *CCAT1-L* RNA accumulates to chromatin regions at or near the *MYC* locus. Double FISH of *egfp-CCAT1-L* (green) with *CCAT1-L* DNA region, *MYC* locus and *MYC*-335 region revealed the co-localization of *egfp-CCAT1-L* with these loci, but not with 15q11-13. Position-specific 10-15 kb probes (shown in **A**) or a probe recognizing15q11-13 [32] were used in DNA FISH. White arrows indicate the single-allele overexpressing *egfp-CCAT1-L* or its co-localized DNA regions in representative cells. **(F)** A schematic drawing of chromatin loops at the *MYC* locus. Loop 1 (pink line) is between the *MYC* promoter (red box) and *MYC*-335 (brown box); loop 2 (blue line) is between *MYC*-335 and *MYC*-515 (green box); the spatially close localization of loop 1 and loop 2 resulted in the chromatin looping between the *MYC* promoter and *MYC*-515, which is "loop 3". In **C** and **E**, a single Z stack of representative images acquired with an Olympus IX70 DeltaVision Deconvolution System microscope is shown. Supportive data are included in Supplementary information, Figure S5.

trol cell lines (Figure 3H). Taken together, we conclude that *CCAT1-L* plays a role in tumorigenesis by positively regulating *MYC* expression *in cis*.

The genomic locus encoding CCAT1-L is spatially close to the MYC locus

How does *CCAT1-L* regulate *MYC* transcription across a distance of 515 kb on 8q24? It is known that chromatin looping can juxtapose genes or enhancers to spatially distant regions [36]. For example, a well-characterized chromatin loop between a locus 335 kb upstream (*MYC*-335) and the *MYC* promoter in CRC was reported, and *MYC*-335 was proposed to act as a transcriptional enhancer for *MYC* [22, 23]. We reasoned that the *CCAT1-L*-transcribing locus *MYC*-515 may also locate close to *MYC* by forming a chromatin loop. By using Chromosome Conformation Capture (3C) to measure the chromatin interaction frequency of a constant fragment at *MYC*-335 with a number of target fragments between the *MYC* promoter and *MYC*-515, we found that the highest interaction frequencies were between *MYC*-335 and the *MYC* promoter, and between *MYC*-335 and *MYC*-515 (Figure 4A). The results were confirmed when a constant fragment was set at *MYC*-515 (Figure 4B) or in the *MYC* promoter (Supplementary information, Figure S5A) in 3C experiments. These results clearly suggest that the genomic locus encoding *CCAT1-L* (*MYC*-515) is spatially close to *MYC* and *MYC*-335 in addition to the known chromatin loop between the *MYC* promoter and *MYC*-335 (Figure 4B).

To further confirm our 3C results, we visualized the localization of the *MYC* promoter and *MYC*-515 by double DNA FISH in single HT29 cells. We designed two short probes (~10 kb in length) that recognize either the *MYC* promoter or *MYC*-515 to achieve a higher resolution for double DNA FISH. The 8q24 region is amplified to at least 6 copies in HT29 cells [37, 38]. We found that on average each probe can detect 6 copies of the *CCAT1* locus and 8 copies of the *MYC* locus in HT29 cells (Figure 4C and 4D). Importantly, 95% of the detected *CCAT1* loci colocalize with *MYC* loci (Figure 4D).

Although CRC-derived cancer cell lines usually contain multiple chromatin copies of 8q24 (Figure 4C and 4D), the *in cis* activated *egfp-CCAT1-L* HCT116 cell line provided a clearer system that allowed us to visualize the localization of *CCAT1-L* with its adjacent chromatin. In agreement with the spatially close localization of *MYC*-515, *MYC*-315 and the *MYC* locus, we found that these three loci, although separated by 515 kb in distance on 8q24, are associated with *CCAT1-L* RNA as revealed by the fact that *in cis* activated *egfp-CCAT1-L* exhibited the strong colocalization with all of these loci (Figure 4E, and a schematic view is shown in Figure 4F). Meanwhile, a control DNA FISH that recognizes 15q11-13 region [32] showed no co-localization with the *in cis* activated *egfp-CCAT1-L*. Taken together, the chromatin organization at the *MYC* locus and the unique localization pattern of *CCAT1-L* strongly support the notion that

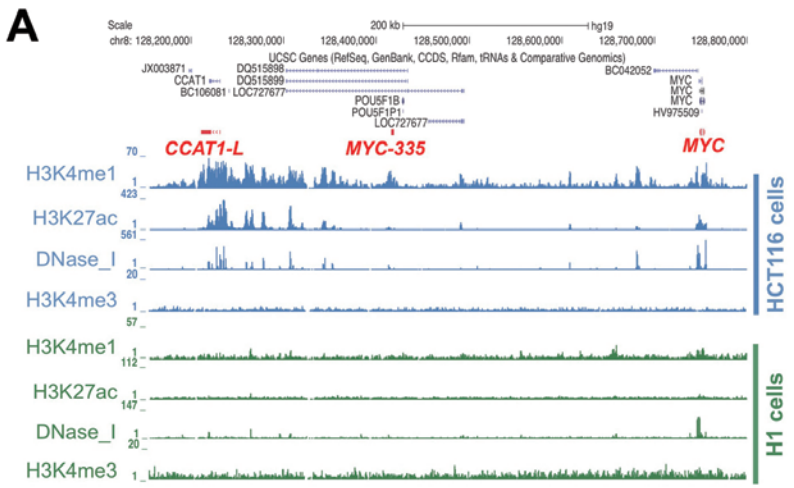
A
CCAT1-L
MYC-335
MYC
H3K4me1
H3K27ac
DNase_I
H3K4me3
HCT116 cells
H1 cells

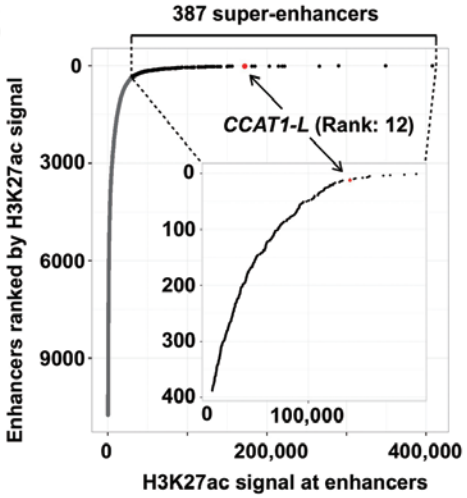
B
387 super-enhancers
CCAT1-L (Rank: 12)
Enhancers ranked by H3K27ac signal
H3K27ac signal at enhancers

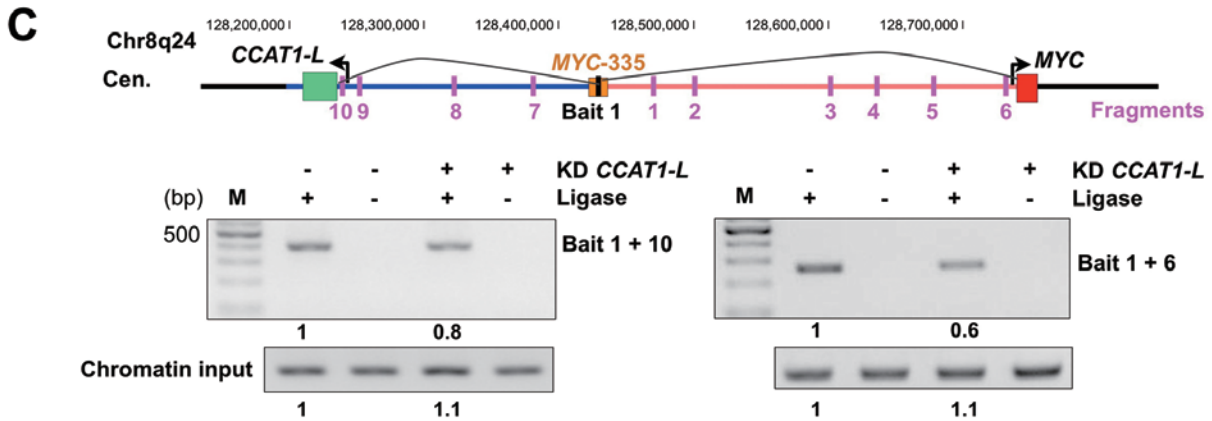
C
Chr8q24
Cen.
CCAT1-L
MYC-335
MYC
Bait 1
Fragments
KD CCAT1-L
Ligase
Bait 1 + 10
Bait 1 + 6
Chromatin input

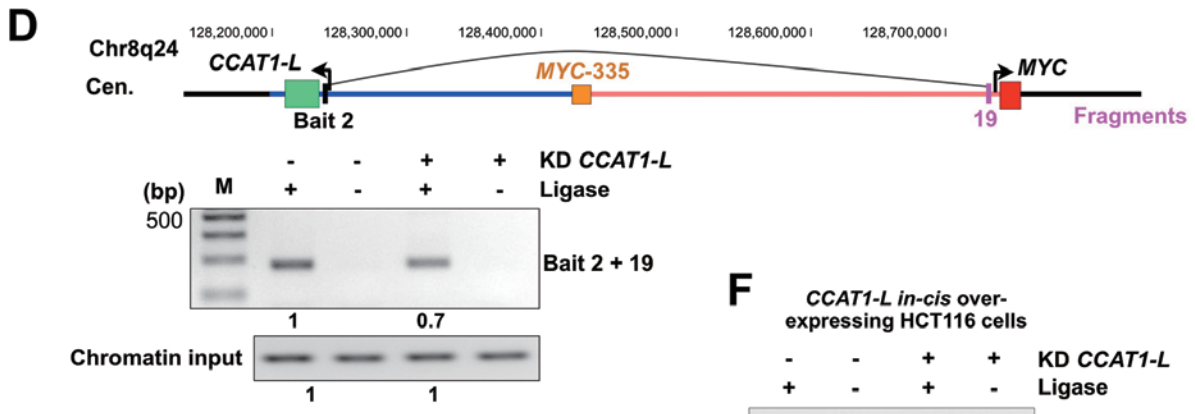
D
Chr8q24
Cen.
CCAT1-L
MYC-335
MYC
Bait 2
Fragments
KD CCAT1-L
Ligase
Bait 2 + 19
Chromatin input

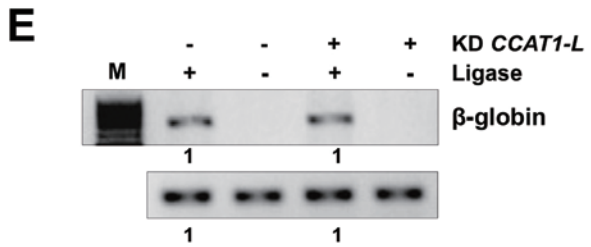
E
KD CCAT1-L
Ligase
β-globin

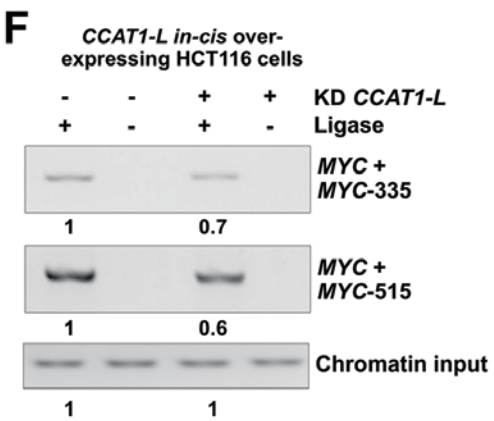
F
CCAT1-L in-cis over-expressing HCT116 cells
KD CCAT1-L
Ligase
MYC + MYC-335
MYC + MYC-515
Chromatin input

Figure 5 *CCAT1-L* is required to maintain the chromatin looping at the *MYC* locus. **(A)** The chromatin region between *MYC*-515 and *MYC*-335 exhibits strong characteristics of a super-enhancer in HCT116 cells but not in H1 cells (histone modifications data were retrieved from ENCODE collection [39]). *CCAT1-L*, *MYC-335* and *MYC* loci are highlighted in red. **(B)** Distribution of H3K27ac signal across enhancers (outer figure) and super-enhancers (inner figure) in HCT116 cells. Rank and H3K27ac signal of enhancers and super-enhancers were downloaded from the literature [20]. 387 super-enhancers (black points) were identified from uneven distribution of H3K27ac signal among normal enhancers (grey points), and the *CCAT1-L*-associated super-enhancer (red point) is ranked as #12 super-enhancers with high H3K27ac signals. **(C**, **D)** Knockdown of *CCAT1-L* reduced the chromatin looping at the *MYC* locus. The long-range interaction frequencies between three chromatin regions (*MYC*-335/*MYC*, *MYC*-335/*MYC*-515, and *MYC*/*MYC*-515) were reduced after knockdown of *CCAT1-L* as revealed by 3C assays in HT29 cells. Over 90% of *CCAT1-L* was depleted after the ASO treatment in 3C assays (data not shown). **(E)** Knockdown of *CCAT1-L* has no effect on the chromatin looping at the β-globin locus. The same *Hind*III restriction fragments were designed for 3C primers and PCRs were performed at the same time as **C** and **D**. **(F)** Knockdown of *CCAT1-L* reduced the chromatin looping at the *MYC* locus in HCT116 cell line with *CCAT1-L in cis* overexpression. The long-range interaction frequencies between the chromatin regions examined in **B** and **C** were also reduced after knockdown of *CCAT1-L* in the HCT116 cell line as revealed by 3C assays. In **C**-**F**, the relative abundance of each 3C PCR product was determined using ImageJ and labeled underneath. 3C experiments were repeated three times. Supportive data are included in Supplementary information, Figures S5 and S6.

CCAT1-L can regulate *MYC* expression *in cis*.

The genomic locus encoding CCAT1-L is a strong super-enhancer

One way to activate gene expression across large distances is by enhancer DNA elements that form long-range chromatin loops with their target genes [9]. Recent genome-wide analyses of chromatin markers in different human cell lines [39] have provided a rich resource to allow us to analyze the chromatin modifications in the *MYC*-515 region. Genome-wide mapping of enhancers in HCT116 cells by searching for locations with high H3K27 acetylation (H3K27ac), high H3K4 mono-methylation (H3K4me1) but low H3K4 tri-methylation (H3K4me3) [40] revealed that the genomic locus encoding *CCAT1-L* is an enhancer that spans up to 150 kb in length (Figure 5A). The size of this enhancer is distinct from that of a typical enhancer which is ~1.5 kb in length on average [17]. Analyzing the distribution of H3K27ac signal across enhancers further revealed that this region is a strong super-enhancer in HCT116 cells [20] (Figure 5B). Also consistent with a role as a super-enhancer, this region is enriched for CBP/P300 binding sites and hypersensitive to DNase I but is devoid of H3K27me3 modification (Figure 5A and data not shown). Moreover, in agreement with the highly cell- or tissue-specific feature of enhancers [9], we found that this enhancer is associated with enhancer-specific histone modifications in CRC cell lines, but not in other cell lines, such as the human embryonic stem cell H1 line (Figure 5A). This is consistent with the very recent report that the gene desert surrounding *MYC* contains tumor type-specific super-enhancers in cancer cells, but not in their healthy counterparts [20].

CCAT1-L is required for the maintenance of chromatin looping at the MYC locus

Recent studies have suggested that a large fraction of enhancers can be bidirectionally transcribed into eRNAs [11] which have been proposed to contribute to gene activation at a distance [12-16], presumably by the establishment or maintenance of enhancer-promoter looping. We asked whether the CRC-specific super-enhancer region-transcribed *CCAT1-L* plays a role in the maintenance of chromatin looping between the *MYC* promoter and its enhancers.

We measured the relative chromatin interaction frequency at the known interaction regions on 8q24 (Figure 4) by 3C experiments before and after knockdown of *CCAT1-L*. Strikingly, we observed that the interaction frequencies between *MYC*-335 and the *MYC* promoter and between *MYC*-335 and *MYC*-515 were significantly reduced after *CCAT1-L* knockdown (Figure 5C). The interaction frequency between *MYC*-515 and the *MYC* promoter was also greatly reduced under the same treatment (Figure 5D). In contrast, another known loop at the β-globin locus was not altered (Figure 5E). Moreover, knockdown of *CCAT1-L* in the *CCAT1-L-in cis* overexpressing cell line also reduced the interaction frequencies between the looping regions upstream of *MYC* (Figure 5F). Importantly, these observations were further supported by 3C-Seq [41] with bait fragment recognizing the *CCAT1-L* locus (*MYC-515*) in control and *CCAT1-L*-depleted cells (Supplementary information, Figure S6). Many long-range chromatin interactions were detected within the 500-kb region between the *CCAT1-L* and *MYC* loci (Supplementary information, Figure S6), which was consistent with available 5C datasets generated by the University of Washington ENCODE GROUP (http://genome.ucsc.edu/cgi-bin/hgTrackUi?db=hg19&g=wg

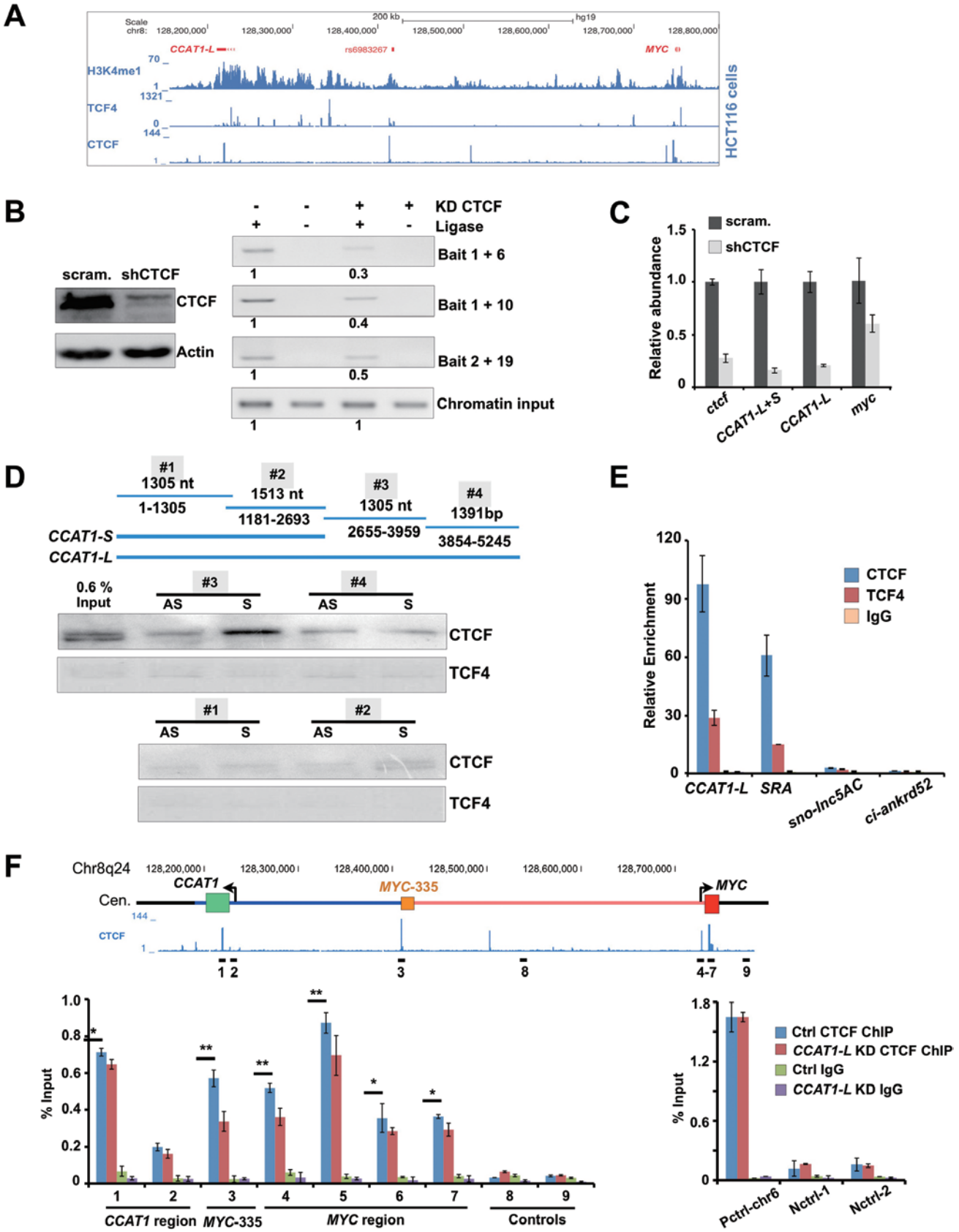
A
Scale
chr8:
128,200,000
128,300,000
128,400,000
128,500,000
128,600,000
128,700,000
128,800,000
200 kb
hg19
CCAT1-L
rs6983267
MYC
H3K4me1
TCF4
CTCF
HCT116 cells
B
KD CTCF
Ligase
scram.
shCTCF
CTCF
Actin
Bait 1 + 6
Bait 1 + 10
Bait 2 + 19
Chromatin input
C
scram.
shCTCF
Relative abundance
ctcf
CCAT1-L+S
CCAT1-L
myc
D
#1
1305 nt
1-1305
#2
1513 nt
1181-2693
#3
1305 nt
2655-3959
#4
1391bp
3854-5245
CCAT1-S
CCAT1-L
0.6 % Input
AS
S
CTCF
TCF4
E
CTCF
TCF4
IgG
Relative Enrichment
CCAT1-L
SRA
sno-lnc5AC
ci-ankrd52
F
Chr8q24
CCAT1
MYC-335
MYC
Cen.
CTCF
% Input
CCAT1 region
MYC-335
MYC region
Controls
Ctrl CTCF ChIP
CCAT1-L KD CTCF ChIP
Ctrl IgG
CCAT1-L KD IgG
Pctrl-chr6
Nctrl-1
Nctrl-2

Figure 6 *CCAT1-L* interacts with CTCF and modulates CTCF binding to chromatin. **(A)** ChIP-seq revealed that TCF4 and CTCF are enriched at 8q24 in HCT116 cells (ChIP-seq data were retrieved from ENCODE collection [39]). **(B)** CTCF is required for chromatin looping at 8q24. Left, knockdown of CTCF was achieved using shRNA against CTCF as confirmed by WB. Right, the long-range interaction frequencies between three chromatin regions (*MYC*-335/*MYC*, *MYC*-335/*MYC*-515, and *MYC*/*MYC*-515, primers used in **Figure 4**) were reduced after knockdown of CTCF as revealed by 3C assays in HT29 cells. The relative abundance of each 3C PCR product was determined using ImageJ and labeled underneath. 3C experiments were repeated for three times. **(C)** CTCF is required for *MYC* and *CCAT1-L* expression. The relative abundance of *MYC* and *CCAT1-L* was analyzed by RT-qPCR in control and CTCF-knockdown HT29 cells. **(D)** *CCAT1-L* and CTCF interact *in vitro*. Top, a schematic view of four overlapping *CCAT1-L* RNA fragments for IVT. Bottom, biotin-labeled RNA pull-down assay using different fragments of *CCAT1-L* transcript in HT29 nuclear extracts showed that one fragment of *CCAT1-L* binding to CTCF. No *CCAT1-L* fragment was specifically associated with TCF4. **(E)** Interaction between endogenous *CCAT1-L* and CTCF was confirmed by RNA immunoprecipitation (RIP). RIP was performed with HT29 cells after UV crosslinking by using anti-CTCF, anti-TCF4 and anti-IgG, followed by RT-qPCR. Bar plots represent fold enrichments of RNAs immunoprecipitated by each indicated antibody over anti-IgG. SRA, steroid receptor RNA activator [54]; sno-lnc5AC, H/ACA sno-lncRNA [32]; ci-ankrd52, a circular intronic RNA [33]. **(F)** *CCAT1-L* modulates CTCF binding to chromatin. Knockdown of *CCAT1-L* reduced the interaction of CTCF to its occupied sites in chromatin. ChIP with anti-CTCF in scramble- and *CCAT1-L* ASO-treated HT29 cells. Data were expressed as the percentage of CTCF co-precipitating DNAs in *MYC* promoter, *MYC*-335, *MYC*-515 regions and negative CTCF binding sites on 8q24, versus input under each indicated condition (left). Control CTCF ChIPs were performed on positive and other negative CTCF binding sites (right). *P* values from one-tailed *t*-test in the pairwise comparison are shown (**P* < 0.05, ***P* < 0.01). In **E** and **F**, error bars represent ± SD in triplicate experiments. Supportive data are included in Supplementary information, Figure S6.

EncodeUw5C). Importantly, loops between *MYC* and *MYC-335*, and between *MYC*-335 and *MYC*-515 were most significantly affected by knockdown of *CCAT1-L* (Supplementary information, Figure S6). Together, these results suggest that the super-enhancer region-transcribed *CCAT1-L* is required for the maintenance of certain chromatin loops at the *MYC* locus in CRC cancer cells. We observed the same phenomenon when the same chromatin loops between the *MYC* promoter and its enhancers were assayed using different sets of "bait" and "fragment" PCR primer sets (data not shown) and in two additional biological repeats (data not shown). In all assays, 3C PCR products were Sanger sequenced to confirm that they mapped to the designed separated chromatin regions with a *Hind*III cutting site (Supplementary information, Figure S5B).

CTCF plays a role in mediating long-range chromatin interactions between the MYC promoter and its enhancers

Analyses of the available ChIP-seq datasets [39] revealed that TCF4 and CTCF are highly enriched in this 8q24 region in HCT116 cells (Figure 6A). Extensive TCF4 binding in the chromatin region between *MYC*-515 and *MYC*-335 was consistent with the notion that this chromatin region is a super-enhancer that can recruit transcriptional factors (Figure 5A). Expression of a dominant-negative TCF4 in HT29 cells resulted in reduced expression of both *MYC* and *CCAT1-L* (Supplementary information, Figure S7A), confirming a role of TCF4 in both *MYC* [42] and *CCAT1-L* regulation, and suggesting that the transcription of *CCAT1-L* is responsive to TCF4 signaling in CRC.

In addition, the specific enrichment of CTCF at sites for chromatin looping formation in the *MYC* promoter, *MYC*-335 and *MYC*-515 regions (Figure 6A) suggests that these chromatin loops observed at the *MYC* locus are CTCF-mediated. It is in agreement with a critical role of CTCF in mediating chromatin looping (rather than only functioning as an "insulator") [43-45]. This is what we have observed for the 8q24 region. Knockdown of CTCF disrupted these chromatin loops, as revealed by reduced chromatin interaction frequencies between the *MYC* promoter and its enhancers (Figure 6B). Importantly, knockdown of CTCF led to reduced expression of *MYC* and *CCAT1-L* (Figure 6C and Supplementary information, Figure S7B), supporting the notion that CTCF and CTCF-mediated chromatin looping are required to maintain proper transcription of both *MYC* and *CCAT1-L*. This also indicates the possibility that CTCF and *CCAT1-L* may participate in a positive regulatory network in control of *MYC* transcription by regulating the higher chromatin organization of 8q24 surrounding the *MYC* locus.

CCAT1-L interacts with CTCF and modulates CTCF binding to chromatin at the MYC locus

As *CCAT1-L* is required for the maintenance of chromatin looping at the *MYC* locus (Figure 5 and Supplementary information, Figure S6), we set up analyses to understand the underlying mechanisms by searching for *CCAT1-L*-interacting proteins using biotin-labeled RNA

pull-down assays. TCF4 and CTCF are enriched at *MYC*-515 (Figure 6A) and it is known that many DNA-binding proteins can also bind to RNAs [46, 47]. As a first step to examine *CCAT1-L*-associated proteins, we asked whether *CCAT1-L* is associated with TCF4 and CTCF.

CCAT1-L is 5 200 nt in length, which is too long to achieve an efficient biotin-labeled *in vitro* transcription (IVT) with a proper folding in denatured buffer (data not shown). Therefore, we generated several sense and antisense biotin-labeled IVT fragments that span the full sequence of *CCAT1-L*, each overlapping another by 100 nt at both ends (Figure 6D). After incubation with nuclear extracts isolated from HT29 cells with individual biotin-labeled RNA fragments, we found that only the sense biotin-labeled 2 655-3 959 fragment of *CCAT1-L*, which does not overlap with *CCAT1-S*, specifically interacted with CTCF (Figure 6D). In contrast, no fragment could specifically bring down TCF4 or another abundant nuclear protein $p54^{nrb}$ (Figure 6D and data not shown), confirming the specificity of this pull-down assay. Furthermore, we confirmed the specific interaction between *CCAT1-L* and CTCF by RNA immunoprecipitation (Figure 6E). We found that *CCAT1-L* was efficiently co-precipitated with antisera directed against CTCF, but much less efficiently with those targeting TCF4 (Figure 6E). Other abundant ncRNAs, *H/ACA* sno-lncRNA [32] or ciRNA [33] , could not be pulled down by these antibodies, demonstrating the specificity of the RNA precipitation assays. Together, these analyses strongly indicate that *CCAT1-L* specifically interacts with CTCF.

We finally asked whether the interaction of *CCAT1-L* and CTCF contributes to the observed role of *CCAT1-L* in the maintenance of the long-range chromatin interactions between the *MYC* promoter and its enhancers (Figures 4, 5 and Supplementary information, Figure S6). Knockdown of *CCAT1-L* led to a modest reduction of CTCF binding to chromatin at their occupied chromatin sites in loop-forming regions at the *MYC* locus (Figure 6F). This suggests that *CCAT1-L* lncRNA may act to locally concentrate CTCF or allosterically modify CTCF binding to chromatin to maintain the chromatin looping in the 8q24 region surrounding the *MYC* locus in CRC cancers. We have consistently observed only modest effects on CTCF binding to chromatin after knockdown of *CCTA1-L*, which is in agreement with the recent report that CTCF-occupied chromatin sites often anchor constitutive chromatin interactions [44].

Discussion

Recent studies reported that many enhancers can bidirectionally express non-polyadenylated noncoding RNAs (eRNAs) with very low copy numbers [11, 48, 49]. Such eRNAs have been proposed to play an enhancer-like role in transcriptional activation at a distance, presumably by the establishment or maintenance of enhancer-promoter looping [12-16]. In addition, AR-associated lncRNAs *PRNCR1* and *PCGEM1* were shown to be involved in the regulation of AR-dependent gene activation events by a sequential recruitment of *PRNCR1* and *PCGEM1* to AR and the recognition of H3K4me3 marks by *PCGEM1*-recruited PYGO2 to enhance interactions of AR-bound enhancers with target gene promoters genome-widely [26]. In the current study, we found that the locus 515 kb upstream of *MYC* is a super-enhancer (Figure 5A and 5B), which is about 150 kb in length and forms chromatin loops with *MYC* (Figures 4, 5, Supplementary information, Figures S5 and S6). Interestingly, it has been very recently highlighted as a tumor type-specific super-enhancer [20]. Our results showed that this *MYC* locus-related super-enhancer (Figure 5A) expresses a human colorectal cancer-specific lncRNA *CCAT1-L* (Figure 1). This lncRNA is polyadenylated and is specifically accumulates *in cis* in the nucleus (Figure 1). It positively regulates *MYC* transcription (Figures 2 and 3) by promoting chromatin interactions between *MYC* and its upstream regulatory elements (Figures 4, 5 and Supplementary information, Figure S6). Different from the reported eRNAs or *PCGEM1* that are associated with components of Mediators, cohesin or chromatin modification enzymes [12-14], or directly open the chromatin accessibility [15], our data suggest that *CCAT1-L* interacts with CTCF and modulates CTCF binding to chromatin to maintain the looping at the *MYC* locus (Figure 6).

CTCF has been proposed to act as one of the master candidates as a global genome organizer to coordinate chromatin structures and regulate gene expression [50]. Recent analyses of CTCF-associated higher-order chromatin structures by ChIA-PET [43] and the long-range interaction landscape of gene promoters by 5C [44, 45] have revealed a primary role of CTCF in mediating chromatin looping, rather than only functioning as an insulator [51]. CTCF is particularly involved in the formation of the intermediate-length chromatin loops at scales of 100 kb-1 Mb in a more constitutive way [44]. Consistent with this notion, we showed here that CTCF plays an important role in *MYC* expression and in mediating 300-550 kb long-range chromatin interactions between enhancers and the *MYC* promoter (Figure 6A-6C). However, importantly, we also observed that the association of CTCF with its occupied chromatin sites was influenced by additional context in cancers, such as the presence of the lncRNA *CCAT1-L* in CRC (Figure 6). CTCF has been shown to bind to RNAs [52-54]. Depletion of RNAs ei-

ther affected its binding to cohesin [54] or altered CTCF binding to chromatin [52]. We found that knockdown of *CCAT1-L* led to the modest reduction of CTCF binding to chromatin (Figure 6F). This observation not only further confirmed that the CTCF-occupied sites at the *MYC* locus are constitutive, but also was consistent with the notion that these chromatin loops at the *MYC* locus are under regulation [19, 20]. However, we do not yet know how precisely CTCF coordinates with *CCAT1-L* to regulate the chromatin looping at the *MYC* locus. Also, it is possible that *CCAT1-L* may interact with other chromatin organizers or modifiers in addition to CTCF.

MYC regulation is extremely complex. The physiologic transcriptional control of this gene still is not fully understood due to the lack of a complete annotation of regulatory elements across different tissue types [21]. Our study presented here, as well as others [19, 20], has demonstrated that the megabase-sized region of gene desert around *MYC* contains many regulatory elements (enhancers and super-enhancers) that form looping interactions with *MYC* in a tissue-/tumor type-specific manner. Thus, the proper chromatin organization of 8q24 gene desert region can be the key to precisely regulate *MYC* transcription under different physiologic conditions. In agreement with this notion, *MYC* transcripts in mice lacking *MYC*-335 were modestly reduced [24]. Knockdown of CTCF led to the reduced interactions between the *MYC* promoter and its enhancers (Figure 6B) and a decreased *MYC* transcription as well (Figure 6C). In addition, knockdown of *CCAT1-L* RNA reduced the enhancer-promoter interactions at the *MYC* locus (Figures 5 and Supplementary information, Figure S6) and *MYC* transcription (Figure 2A-2C). The *in cis* overexpression of this lncRNA promoted *MYC* transcription and enhanced tumorigenesis (Figure 3 and Supplementary information, Figure S4), presumably by modulating enhancer-promoter interactions (Figure 5 and Supplementary information, Figure S6). Thus, we propose that the expression of *CCAT1-L* RNA may influence the chromatin organization of 8q24 at the *MYC* locus, contributing in part to the aberrant expression of *MYC* in human colorectal cancer pathogenesis. However, as it has been reported that transcriptional recruitment at certain locus may affect the expression of adjacent genes [55], we do not exclude the possibility that the acquirement of the transcription activity in the *CCAT1-L* locus during CRC pathogenesis may also contribute to the regulation of *MYC* transcription.

Although we do not know to what extent *CCAT1-L*-regulated looping cross-talks with other aspects of *MYC* regulation, this study represents yet another component of the complicated *MYC* region. Finally, as this region also expresses distinct lncRNAs in other types of human cancers, it will be of interest to learn whether other 8q24 lncRNAs behave in a similar way in *MYC* transcription in different cancers.

Materials and Methods

Cell culture and ASO treatment

Human cell lines were cultured using standard protocols provided by ATCC. Phosphorothioate-modified oligodeoxynucleotide (ASO) were synthesized at BioSune, Shanghai, China. The ASO was introduced into HT29 or HCT116 cells by nucleofection (Lonza) according to the manufacturer's protocol. The scramble- and ASO-treated cells were collected for the following experiments.

Total RNA isolation, human tissue RNA samples, RT-PCR, RT-qPCR and northern blot

Total RNAs from cultured cells with different treatments were extracted with Trizol Reagent (Invitrogen). Twenty human tissue RNA samples were purchased from Ambion. For RT-PCR, after treatment with DNase I (Ambion, DNA-free TM kit), the cDNA was transcribed with SuperScript II (Invitrogen), followed by PCR. For qPCR, the relative expression of genes was quantified to actin mRNA from three independent experiments. Primers for PCR and qPCR are listed in Supplementary information, Table S2. For northern blot, equal amounts of total RNAs collected from cultured cells and primary tissue samples from patients were resolved on 1.5% agarose gels and northern blot was carried out as described previously [33]. Digoxigenin-labeled antisense *CCAT1-L* probe and *egfp* probe were made using either SP6 or T7 RNA polymerases by IVT with the DIG Northern Starter Kit (Roche). Primers for northern blot probes are listed in Supplementary information, Table S2.

Patient samples and RNA extractions from tissues and deep sequencing for gene expression analysis

Human paired CRC/control mucosa samples were obtained from Changzheng Hospital, Shanghai under the strict guidance of ethical committee. After frozen tissue samples were powdered in liquid nitrogen, Trizol was added to extract RNA. RNA quality was examined by gel electrophoresis and only paired RNA with high quality was used for following analyses, including RNA-seq. RNA-seq libraries were prepared according to the manufacturer's instructions and then applied to sequencing on Illumina HiSeq 2000 in CAS-MPG Partner Institute for Computational Biology Omics Core, Shanghai and Genergy, Shanghai. In all, 52 and 59 million 1 × 100 single reads of the paired CRC/control mucosa RNA samples were obtained and were uniquely mapped to the hg19 genome with over 85% of mapping rates for both cases. The gene expression analysis was carried out as described previously [32] and genes (mRNAs and lncRNAs) altered significantly in both samples are listed in Supplementary information, Table S1.

Nuclear/cytoplasmic RNA fractionation, nuclear soluble/insoluble RNA fractionation and polyadenylated/non-polyadenylated RNA separation

Nuclear and cytoplasmic RNA isolation in HT29 cells, nuclear soluble and insoluble RNA fractionation were performed as de-

scribed before [32]. Polyadenylated and non-polyadenylated RNA separation in HT29 cells was carried out as described previously in HeLa cells [56]. Semi-quantitative RT-PCR was then used to evaluate the relative abundance of both *CCAT1*s, *XIST* and *actin* in each sample.

RNA ISH and immunofluorescence microscopy

To detect *CCAT1-L* and *CCAT1-S*, RNA ISH was carried out as previously described with *in vitro* transcribed digoxigenin-labeled antisense probes [32]. For colocalization studies, cells were co-stained with rabbit anti-Nucleolin (Santa Cruz Biotechnology), mouse anti-p54^{nrb} (BD) and mouse anti-Coilin (Sigma). The nuclei were counterstained with DAPI. Images were taken with a Zeiss LSM 510 microscope or with an Olympus IX70 DeltaVision RT Deconvolution System microscope.

RNA/DNA double FISH

Sequential RNA/DNA double FISH experiments were carried out as described previously [32]. After RNA ISH, cells were denatured at 80 °C for 5 min in prewarmed 2× SSC and 70% deionized formamide, pH 7.0. Next, cells were hybridized with denatured labeled DNA probe prepared by Nick Translation (Empire Genomics) overnight. After hybridization, two washes of 10 min at 37 °C with 2× SSC/50% deionized formamide, pH 7.0, followed by two washes of 15 min at 37 °C with 1× SSC and two washes of 15 min at 37 °C with 2× SSC were performed. Slides were then mounted with ProLong Gold antifade reagent with DAPI. Analyses were performed on single Z stacks acquired with an Olympus IX70 DeltaVision RT Deconvolution System microscope. Colocalization signals were detected in > 95% double-positive cells.

Double DNA FISH and statistical analyses

Double DNA FISH experiments were carried out as described above with minor modifications. Position-specific 10-15 kb probes were amplified by long-range PCR directly from genomic DNAs with primers listed in Supplementary information, Table S2. These DNA FISH probes that target the specific looping interactions of 8q24 were labeled with Alexa Fluor 488 (green) or 594 (red) by Nick Translation (Empire Genomics). After fixation and permeabilization, cells were denatured at 80 °C for 5 min in prewarmed 2× SSC and 70% deionized formamide pH 7.0. Next, cells were hybridized overnight at 37 °C with denatured labeled DNA probes. After hybridization, two washes of 10 min at 37 °C with 2× SSC/50% deionized formamide, pH 7.0, followed by two washes of 15 min at 37 °C with 1× SSC and two washes of 15 min at 37 °C with 2× SSC were performed. Slides were then mounted with ProLong Gold antifade reagent with DAPI. Pictures were taken with an Olympus IX70 DeltaVision RT Deconvolution System microscope. Colocalization signals were analyzed in double-positive cells.

UV crosslinking RNA immunoprecipitation

UV crosslinking RIP was carried out as described before [33]. Two 10 cm^2 dishes of HT29 cells with 90%-100% confluence were washed twice with 5 ml cold PBS and irradiated at 300 mJ/cm^2 at 254 nm in a Stratalinker. Cells were collected and resuspended in 1 ml RIP buffer (50 mM Tris-HCl, pH 7.5, 150 mM NaCl, 1% NP-40, 0.5% sodium deoxycholate, 1 mM PMSF, 2 mM VRC, protease inhibitor cocktail). Then cells were homogenized by 3 rounds of sonication on ice. Insoluble material was removed by centrifugation and the supernatant was pre-cleared with Dynabeads G (Invitrogen) with 20 μg/ml yeast tRNA at 4 °C for 30 min. The pre-cleared lysate was incubated with Dynabeads G that were pre-coated with 2 μg antibodies of anti-CTCF (Millipore), anti-TCF4 (Millipore) or IgG (Sigma) for 4 h at 4 °C. The beads were washed sequentially with washing buffer I (50 mM Tris-HCl, pH 7.5, 1 M NaCl, 1% NP-40, 1% sodium deoxycholate, 2 mM VRC) and washing buffer II (50 mM Tris-HCl, pH 7.5, 1 M NaCl, 1% NP-40, 1% sodium deoxycholate, 2 mM VRC, 1 M urea) for multiple times. The immunoprecipitated complex was eluted from Dynabeads G by adding 140 μl elution buffer (100 mM Tris-HCl, pH 7.0, 5 mM EDTA, 10 mM DTT, 1% SDS). 5 μl of 10 mg/ml proteinase K was then added to the retrieved RNA samples and incubated at 55 °C for 30 min, followed by RNA extraction and qPCR.

Chromatin immunoprecipitation (ChIP)

1×10^7 cultured cells with each treatment were washed with ice-cold PBS, crosslinked with 1% formaldehyde and quenched by 0.125 M glycine. After being resuspended with 1 ml ChIP lysis buffer (1% Triton X-100, 0.1% sodium deoxycholate, 50 mM Tris, pH 8.0, 150 mM NaCl, 5 mM EDTA), cells were sonicated to achieve the majority of DNA fragments with 200-500 bp. Supernatants were collected and pre-cleared with Dynabeads G in ChIP lysis buffer with the supplement of 100 μg BSA and 100 μg ssDNA. Then, the pre-cleared cell lysates were used for ChIP with 2 μg CTCF antibody (Millipore) for overnight incubation at 4 °C. The beads were then washed with 600 μl ChIP lysis buffer, 600 μl high salt wash buffer (1% Triton X-100, 0.1% deoxycholate, 50 mM Tris, pH 8.0, 500 mM NaCl, 5 mM EDTA), 600 μl of LiCl immune complex wash buffer (0.25 M LiCl, 0.5% Igepal, 0.5% deoxycholate, 10 mM Tris, pH 8.0, 1 mM EDTA), followed by two washes with 600 μl 1× TE Buffer (10 mM Tris, pH 8.0, 1 mM EDTA) at 4 °C. The immunoprecipitated complex was eluted from Dynabeads G by adding 200 μl fresh-prepared elution buffer (1% SDS, 0.1 M $NaHCO_3$) with rotation at room temperature (RT) for 15 min. Then the reverse crosslinking was carried out by adding 8 μl of 5 M NaCl and incubating at 65 °C for 4 h, followed by incubating with the supplement of 4 μl of 0.5 M EDTA and 10 μl proteinase K (10 mg/ml) at 55 °C for 2 h. DNA was recovered by phenol/chloroform extraction and ethanol precipitation, followed by qPCR with the primers listed in Supplementary information, Table S2.

Biotin-labeled RNA pull-down assay

Biotin-labeled RNAs pull-down assay was performed as described [33, 57, 58] with minor modifications. Biotin-labeled *CCAT1-L* truncation probes were *in vitro* transcribed with the Biotin RNA Labeling Mix (Roche) and AmpliScripe T7/SP6-flash Transcription Kit (Epicentre). 4 μg biotinylated RNA was denatured for 5 min at 65 °C in PA buffer (10 mM Tris-HCl, pH 7.5, 10 mM $MgCl_2$, 100 mM NH_4Cl) and slowly cooled down to RT. 2×10^7 HT29 cell pellet was used for each assay. Briefly, HT29 cell nuclei [33] were resuspended in 1 ml RIP buffer (25 mM Tris-HCl, pH 7.5, 150 mM KCl, 0.5 mM DTT, 0.5% NP-40, 1 mM PMSF, 2 mM VRC, protease inhibitor cocktail). The nuclei were sonicated on ice followed by centrifugation at 13 000 rpm for 10 min at 4 °C. The supernatant was transferred to a new tube and pre-cleared by applying 40 μl Streptavidin Dynabeads for 20 min at 4 °C. Then

20 μg/ml yeast tRNA was added to block nonspecific binding and incubated for 20 min at 4 °C. Folded RNAs were then added and incubated for 1.5 h at RT, followed by the addition of 40 μl Streptavidin Dynabeads to incubate for 1.5 h. Beads were washed with RIP buffer containing 0.5% sodium deoxycholate and denatured in 1× SDS loading buffer. The retrieved proteins were analyzed by western blot with anti-CTCF (Millipore) and anti-TCF4 (Millipore) antibodies.

Nuclear run-on (NRO)

The NRO assay in HT29 cells was performed as described previously [33] with minor modifications. In brief, HT29 cells were washed with cold PBS quickly and collected for NRO assay 24 h post nucleofection with ASOs. Collected cells were incubated in swelling buffer (10 mM Tris, pH 7.5, 2 mM $MgCl_2$, 3 mM $CaCl_2$) on ice for 5 min and were then collected by centrifugation. Cell pellets were subjected to lysis twice with 1.5 ml lysis buffer (10 mM Tris, pH 7.5, 2mM $MgCl_2$, 3 mM $CaCl_2$, 0.5% Igepal, 10% glycerol, and 2 U/ml RNasin Ribonuclease Inhibitor) to obtain purer nuclei. The resulting nuclear pellets were resuspended in 100 μl NRO buffer (50 mM Tris, pH 7.5, 5 mM $MgCl_2$, 150 mM KCl, 0.1% sarkosyl, 2 U/ml RNase inhibitor and 10 mM DTT) containing 0.1 mM ATP, GTP, CTP and BrUTP (Sigma). Transcription was performed for 3 min on ice and then 5 min at RT. The reaction was stopped by addition of 600 μl Trizol to extract RNA, followed by the DNase I (Ambion, DNA-free TM kit) treatment to remove genomic DNA. Purified RNAs were incubated with 2 μg anti-BrdU antibody (Sigma) or equal amount of IgG antibody (Sigma) at 4 °C for 2 h and were then immunoprecipitated with Dynabeads G pre-coated with yeast tRNA (Sigma). Precipitated RNAs were extracted by Trizol and were used for cDNA synthesis and qPCR analysis.

Chromosome conformation capture (3C)

3C was performed as described [59] with modifications. HT29 cells and HT29 cells under different treatments were crosslinked with 1% formaldehyde for 10 min at RT, followed by quenching the crosslinking with addition of 0.125 M glycine. The nuclei were collected and dounced in lysis buffer, followed by adding 400 U of *Hind*III restriction enzyme for overnight digestion at 37 °C with shaking. Ligation was performed for 4 h at 16 °C followed by 1 h incubation with 50 U of T4 DNA ligase at RT. Reverse crosslinking was performed in the presence of proteinase K overnight at 65 °C. The genomic DNA was then extracted by phenol-chloroform. After RNase A treatment, the genomic DNA was qualified with an input primer to balance the input chromatin across different samples. After normalization with input, equal amount of chromatin DNA was used in each PCR reaction to identify the chromatin loops and to compare the alterations between the targeted chromatin loops under different treatments. All 3C primers were designed according to a previous report [60] and listed in Supplementary information, Table S2. The PCR products with expected sizes were Sanger sequenced to ensure that a specific product is exactly the sequence of the ligation event. The 3C control chromatin loop (β-globin) was also examined in the same way as described above.

3C Sequencing

The 3C-Seq libraries were prepared step by step as described by Stadhouders R *et al*. [41]. *Hind*III and *Dpn*II were used as the primary and secondary restriction endonuclease. The 3C-Seq library was sequenced (70 bp reads) with Illumina HiSeq 2000. The 3C sequencing signals were normalized with both the total sequencing reads and the highest frequency signal nearby the bait primer. The relative signals were shown in a "*CCAT1*-to-*MYC*" viewpoint in Supplementary information, Figure S6.

In cis overexpression of CCAT1-L or EGFP with TALEN

All TALENs were designed and assembled according to literature [61]. The TALEN assembly kit was obtained from Addgene. The target sequence of *CCAT1-L* TALEN is TCATCATTACCAGCTGCCGT and TTTCTGTGAATCGTGAGCGT. The homologous arm sequences for donor plasmids are chr8: 128231306-128232194 and chr8: 128230503-128231297. After insertion of the homologous arms amplified from the genomic DNA of HCT116 cells into pCRII vector (backbone for Donor plasmid construction), the different regulatory modules (*CMV*/*Puro*/*egfp* and the *BGH*/*SV40* poly(A) sites) were amplified from commercially available expression vectors including pEGFP-C1 and pLKO.1, followed by the insertion into the donor plasmid by overlapping PCRs to obtain desired TALEN vectors (Figure 3C and Supplementary information, Figure S4A). All plasmids were validated by Sanger sequencing. After transfection of individual sets of TALEN vectors and donor plasmids into HCT116 cells, puromycin was added to facilitate positive single clone screening. Genomic DNAs of selected single clones were extracted for the genotyping validation with appropriate sets of primers listed in Supplementary information, Table S2. The positive clones were scaled up for banking and detailed experiments (Figures 3, Supplementary information, Figures S4 and S5).

Tumor xenograft assay

Female nude mice between 4 and 6 weeks were obtained from SLAC laboratory animal company and bred in SPF animal house. All animal work was done in accordance with a protocol approved by the Shanghai Experimental Animal Center (Chinese Academy of Sciences). After 1 week feeding after reaching the animal house, mice were inoculated subcutaneously with 3-4 × 10^6 indicated cells of individual TALEN-engineered cell lines. Mice were maintained in SPF animal house and were sacrificed for tumor weight analyses when the xenografts reached about 1.5 cm in diameter (at 4 weeks).

Accession numbers

Raw sequencing dataset and bigWig track file of paired human CRC/control mucosa samples and 3C-Seq datasets are available for download from NCBI Gene Expression Omnibus under accession numbers GSE55259 and GSE55261.

Acknowledgments

We thank Drs G Wei and R Stadhouders for assistance in 3C and 3C-seq experiments; Dr GG Carmichael for critical reading of the manuscript; Drs L Li, H Yao, YA Zeng and G Wang for materials; YJ Jiang, H Wu, S Zhu for technical support; and all other lab members for helpful discussion. This work was supported by the Ministry of Science and Technology of China (2014CB964800 and 2014CB910600), the National Natural Science Foundation of China (31271376 and 31322018), and the Shanghai Institutes for

Biological Sciences, Chinese Academy of Sciences (2012OHTP08 and 2012SSTP01).

References

1 Rinn JL, Chang HY. Genome regulation by long noncoding RNAs. *Annu Rev Biochem* 2012; **81**:145-166.
2 Ulitsky I, Bartel DP. lincRNAs: genomics, evolution, and mechanisms. *Cell* 2013;**154**:26-46.
3 Gutschner T, Diederichs S. The hallmarks of cancer: a long non-coding RNA point of view. *RNA Biol* 2012; **9**:703-719.
4 Gupta RA, Shah N, Wang KC, *et al*. Long non-coding RNA HOTAIR reprograms chromatin state to promote cancer metastasis. *Nature* 2010; **464**:1071-1076.
5 Huarte M, Guttman M, Feldser D, *et al*. A large intergenic noncoding RNA induced by p53 mediates global gene repression in the p53 response. *Cell* 2010; **142**:409-419.
6 Yoon JH, Abdelmohsen K, Srikantan S, *et al*. LincRNA-p21 suppresses target mRNA translation. *Mol Cell* 2012; **47**:648-655.
7 Gutschner T, Hammerle M, Eissmann M, *et al*. The noncoding RNA MALAT1 is a critical regulator of the metastasis phenotype of lung cancer cells. *Cancer Res* 2013; **73**:1180-1189.
8 Tripathi V, Shen Z, Chakraborty A, *et al*. Long noncoding RNA MALAT1 controls cell cycle progression by regulating the expression of oncogenic transcription factor B-MYB. *PLoS Genet* 2013; **9**:e1003368.
9 Bulger M, Groudine M. Functional and mechanistic diversity of distal transcription enhancers. *Cell* 2011; **144**:327-339.
10 Orom UA, Shiekhattar R. Long noncoding RNAs usher in a new era in the biology of enhancers. *Cell* 2013; **154**:1190-1193.
11 Kim TK, Hemberg M, Gray JM, *et al*. Widespread transcription at neuronal activity-regulated enhancers. *Nature* 2010; **465**:182-187.
12 Lai F, Orom UA, Cesaroni M, *et al*. Activating RNAs associate with Mediator to enhance chromatin architecture and transcription. *Nature* 2013; **494**:497-501.
13 Lam MT, Cho H, Lesch HP, *et al*. Rev-Erbs repress macrophage gene expression by inhibiting enhancer-directed transcription. *Nature* 2013; **498**:511-515.
14 Li W, Notani D, Ma Q, *et al*. Functional roles of enhancer RNAs for oestrogen-dependent transcriptional activation. *Nature* 2013; **498**:516-520.
15 Mousavi K, Zare H, Dell'orso S, *et al*. eRNAs promote transcription by establishing chromatin accessibility at defined genomic loci. *Mol Cell* 2013; **51**:606-617.
16 Orom UA, Derrien T, Beringer M, *et al*. Long noncoding RNAs with enhancer-like function in human cells. *Cell* 2010; **143**:46-58.
17 Loven J, Hoke HA, Lin CY, *et al*. Selective inhibition of tumor oncogenes by disruption of super-enhancers. *Cell* 2013; **153**:320-334.
18 Whyte WA, Orlando DA, Hnisz D, *et al*. Master transcription factors and mediator establish super-enhancers at key cell identity genes. *Cell* 2013; **153**:307-319.
19 Ahmadiyeh N, Pomerantz MM, Grisanzio C, *et al*. 8q24 prostate, breast, and colon cancer risk loci show tissue-specific long-range interaction with *MYC*. *Proc Natl Acad Sci USA* 2010; **107**:9742-9746.
20 Hnisz D, Abraham BJ, Lee TI, *et al*. Super-enhancers in the control of cell identity and disease . *Cell* 2013; **155**:934-947.
21 Levens D. How the *c-myc* promoter works and why it sometimes does not. *J Natl Cancer Inst Monogr* 2008; **39**:41-43.
22 Pomerantz MM, Ahmadiyeh N, Jia L, *et al*. The 8q24 cancer risk variant rs6983267 shows long-range interaction with MYC in colorectal cancer. *Nat Genet* 2009; **41**:882-884.
23 Tuupanen S, Turunen M, Lehtonen R, *et al*. The common colorectal cancer predisposition SNP rs6983267 at chromosome 8q24 confers potential to enhanced Wnt signaling. *Nat Genet* 2009; **41**:885-890.
24 Sur IK, Hallikas O, Vaharautio A, *et al*. Mice lacking a *Myc* enhancer that includes human SNP rs6983267 are resistant to intestinal tumors. *Science* 2012; **338**:1360-1363.
25 Chung S, Nakagawa H, Uemura M, *et al*. Association of a novel long non-coding RNA in 8q24 with prostate cancer susceptibility. *Cancer Sci* 2011; **102**:245-252.
26 Yang L, Lin C, Jin C, *et al*. lncRNA-dependent mechanisms of androgen-receptor-regulated gene activation programs. *Nature* 2013; **500**:598-602.
27 Nissan A, Stojadinovic A, Mitrani-Rosenbaum S, *et al*. Colon cancer associated transcript-1: a novel RNA expressed in malignant and pre-malignant human tissues. *Int J Cancer J* 2012; **130**:1598-1606.
28 Alaiyan B, Ilyayev N, Stojadinovic A, *et al*. Differential expression of colon cancer associated transcript1 (CCAT1) along the colonic adenoma-carcinoma sequence. *BMC Cancer* 2013; **13**:196.
29 Ling H, Spizzo R, Atlasi Y, *et al*. CCAT2, a novel noncoding RNA mapping to 8q24, underlies metastatic progression and chromosomal instability in colon cancer. *Genome Res* 2013; **23**:1446-1461.
30 Augui S, Nora EP, Heard E. Regulation of X-chromosome inactivation by the X-inactivation centre. *Nat Rev Genet* 2011; **12**:429-442.
31 Kam Y, Rubinstein A, Naik S, *et al*. Detection of a long noncoding RNA (CCAT1) in living cells and human adenocarcinoma of colon tissues using FIT-PNA molecular beacons. *Cancer Letters* 2013 Feb 14. doi: 10.1016/j.canlet.2013.02.014
32 Yin QF, Yang L, Zhang Y, *et al*. Long noncoding RNAs with snoRNA ends. *Mol Cell* 2012; **48**:219-230.
33 Zhang Y, Zhang XO, Chen T, *et al*. Circular intronic long noncoding RNAs. *Mol Cell* 2013; **51**:792-806.
34 Gaj T, Gersbach CA, Barbas CF 3rd. ZFN, TALEN, and CRISPR/Cas-based methods for genome engineering. *Trends Biotechnol* 2013; **31**:397-405.
35 Gutschner T, Baas M, Diederichs S. Noncoding RNA gene silencing through genomic integration of RNA destabilizing elements using zinc finger nucleases. *Genome Res* 2011; **21**:1944-1954.
36 Maston GA, Evans SK, Green MR. Transcriptional regulatory elements in the human genome. *Annu Rev Genom Hum Genet* 2006; **7**:29-59.
37 Corzo C, Petzold M, Mayol X, *et al*. RxFISH karyotype and MYC amplification in the HT-29 colon adenocarcinoma cell line. *Genes Chromosomes Cancer* 2003; **36**:425-426.
38 Kawai K, Viars C, Arden K, *et al*. Comprehensive karyotyping of the HT-29 colon adenocarcinoma cell line. *Genes Chromo-*

somes Cancer 2002; **34**:1-8.
39 Consortium EP, Bernstein BE, Birney E, *et al*. An integrated encyclopedia of DNA elements in the human genome. *Nature* 2012; **489**:57-74.
40 Ong CT, Corces VG. Enhancer function: new insights into the regulation of tissue-specific gene expression. *Nat Rev Genet* 2011; **12**:283-293.
41 Stadhouders R, Kolovos P, Brouwer R, *et al*. Multiplexed chromosome conformation capture sequencing for rapid genome-scale high-resolution detection of long-range chromatin interactions. *Nat Protoc* 2013; **8**:509-524.
42 He TC, Sparks AB, Rago C, *et al*. Identification of c-MYC as a target of the APC pathway. *Science* 1998; **281**:1509-1512.
43 Handoko L, Xu H, Li G, *et al*. CTCF-mediated functional chromatin interactome in pluripotent cells. *Nat Genet* 2011; **43**:630-638.
44 Phillips-Cremins JE, Sauria ME, Sanyal A, *et al*. Architectural protein subclasses shape 3D organization of genomes during lineage commitment. *Cell* 2013; **153**:1281-1295.
45 Sanyal A, Lajoie BR, Jain G, Dekker J. The long-range interaction landscape of gene promoters. *Nature* 2012; **489**:109-113.
46 Burdach J, O'Connell MR, Mackay JP, Crossley M. Two-timing zinc finger transcription factors liaising with RNA. *Trends Biochem Sci* 2012; **37**:199-205.
47 Cassiday LA, Maher LJ 3rd. Having it both ways: transcription factors that bind DNA and RNA. *Nucleic Acids Res* 2002; **30**:4118-4126.
48 De Santa F, Barozzi I, Mietton F, *et al*. A large fraction of extragenic RNA pol II transcription sites overlap enhancers. *PLoS Biol* 2010; **8**:e1000384.
49 Hah N, Murakami S, Nagari A, Danko CG, Kraus WL. Enhancer transcripts mark active estrogen receptor binding sites. *Genome Res* 2013; **23**:1210-1223.
50 Phillips JE, Corces VG. CTCF: master weaver of the genome. *Cell* 2009; **137**:1194-1211.
51 Herold M, Bartkuhn M, Renkawitz R. CTCF: insights into insulator function during development. *Development* 2012; **139**:1045-1057.
52 Sun S, Del Rosario BC, Szanto A, *et al*. Jpx RNA activates Xist by evicting CTCF. *Cell* 2013; **153**:1537-1551.
53 Taft RJ, Hawkins PG, Mattick JS, Morris KV. The relationship between transcription initiation RNAs and CCCTC-binding factor (CTCF) localization. *Epigenet Chromatin* 2011; **4**:13.
54 Yao H, Brick K, Evrard Y, *et al*. Mediation of CTCF transcriptional insulation by DEAD-box RNA-binding protein p68 and steroid receptor RNA activator SRA. *Genes Dev* 2010; **24**:2543-2555.
55 Zhang B, Arun G, Mao YS, *et al*. The lncRNA Malat1 is dispensable for mouse development but its transcription plays a cis-regulatory role in the adult. *Cell Rep* 2012; **2**:111-123.
56 Yang L, Duff MO, Graveley BR, Carmichael GG, Chen LL. Genomewide characterization of non-polyadenylated RNAs. *Genome Biol* 2011;**12**:R16.
57 Klattenhoff CA, Scheuermann JC, Surface LE, *et al*. Braveheart, a long noncoding RNA required for cardiovascular lineage commitment. *Cell* 2013; **152**:570-583.
58 Tsai MC, Manor O, Wan Y, *et al*. Long noncoding RNA as modular scaffold of histone modification complexes. *Science* 2010; **329**:689-693.
59 Hagege H, Klous P, Braem C, *et al*. Quantitative analysis of chromosome conformation capture assays (3C-qPCR). *Nat Protoc* 2007; **2**:1722-1733.
60 Dostie J, Dekker J. Mapping networks of physical interactions between genomic elements using 5C technology. *Nat Protoc* 2007; **2**:988-1002.
61 Cermak T, Doyle EL, Christian M, *et al*. Efficient design and assembly of custom TALEN and other TAL effector-based constructs for DNA targeting. *Nucl Acids Res* 2011; **39**:e82.

(**Supplementary information** is linked to the online version of the paper on the *Cell Research* website.)